NASA TECHNICAL MEMORANDUM

NASA TM X- 72680

NASA TM X- 72680

DYNAMIC-STABILITY TESTS OF AN AIRCRAFT ESCAPE MODULE AT MACH NUMBERS FROM 0.40 TO 2.16

By Edwin E. Davenport and Robert A. Kilgore

April 16, 1975

(NASA-TM-X-72680) DYNAMIC-STABILITY TESTS ON AN AIRCRAFT ESCAPE MODULE AT MACH NUMBERS FROM 0.40 TO 2.16 Final Report (NASA) 58 p HC $4.25 CSCL 01C

N75-21270

Unclas G3/05 13417

NATIONAL AERONAUTICS AND SPACE ADMINISTRATION

LANGLEY RESEARCH CENTER, HAMPTON, VIRGINIA 23665

1. Report No.	2. Government Accession No.	3. Recipient's Catalog No.
NASA TM X-72680		

4. Title and Subtitle	5. Report Date
DYNAMIC-STABILITY TESTS OF AN AIRCRAFT ESCAPE MODULE AT MACH NUMBERS FROM 0.40 TO 2.16	April 16, 1975
	6. Performing Organization Code

7. Author(s)	8. Performing Organization Report No.
Edwin E. Davenport and Robert A. Kilgore	

9. Performing Organization Name and Address	10. Work Unit No.
NASA Langley Research Center Hampton, Virginia 23665	505-11-21-02
	11. Contract or Grant No.

12. Sponsoring Agency Name and Address	13. Type of Report and Period Covered
National Aeronautics and Space Administration Washington, D. C. 20546	Technical Memorandum
	14. Sponsoring Agency Code

15. Supplementary Notes

Final release of special information not suitable for formal publication.

16. Abstract

Wind-tunnel measurements of the aerodynamic damping and oscillatory stability of a model of a proposed escape module for a military aircraft have been made using a small-amplitude forced-oscillation technique in pitch and yaw at Mach numbers from 0.40 to 2.16 and in roll at Mach numbers from 0.40 to 1.20. The results in pitch indicate regions in the angle-of-attack range where the model exhibits large and rapid changes in both damping and stability with angle of attack, probably caused by vortex flow over the fins. There was no pronounced effect of change in angle of attack on damping in yaw. Except for the highest Mach number, negative damping in roll was produced at high negative angles of attack.

17. Key Words (Suggested by Author(s)) (STAR category underlined)	18. Distribution Statement
Aerodynamics Dynamic Stability	Unclassified-Unlimited

19. Security Classif. (of this report)	20. Security Classif. (of this page)	21. No. of Pages	22. Price*
Unclassified	Unclassified	55	$4.25

*Available from { The National Technical Information Service, Springfield, Virginia 22151
STIF/NASA Scientific and Technical Information Facility, P.O. Box 33, College Park, MD 20740

NATIONAL AERONAUTICS AND SPACE ADMINISTRATION

DYNAMIC-STABILITY TESTS OF AN AIRCRAFT ESCAPE MODULE AT MACH NUMBERS FROM 0.40 to 2.16

By Edwin E. Davenport and Robert A. Kilgore
Langley Research Center
Hampton, Virginia

ABSTRACT

Wind-tunnel measurements of the aerodynamic damping and oscillatory stability of a model of a proposed escape module for a military aircraft have been made using a small-amplitude forced-oscillation technique in pitch and yaw at Mach numbers from 0.40 to 2.16 and in roll at Mach numbers from 0.40 to 1.20. The results in pitch indicate regions in the angle-of-attack range where the model exhibits large and rapid changes in both damping and stability with angle of attack, probably caused by vortex flow over the fins. There was no pronounced effect of change in angle of attack on damping in yaw. Except for the highest Mach number, negative damping in roll was produced at high negative angles of attack.

SUMMARY

Wind-tunnel measurements of the aerodynamic damping and oscillatory stability of a model of a proposed escape module for a military aircraft have been made using a small-amplitude forced-oscillation technique in pitch and yaw at Mach numbers from 0.40 to 2.16 and in roll at Mach numbers from 0.40 to 1.20.

The results in pitch indicate regions in the angle-of-attack range where the model exhibits large and rapid changes in both damping and stability with angle of attack, probably caused by vortex flow over the fins. There was no pronounced effect of change in angle of attack on damping in yaw. Except for the highest Mach number, negative damping in roll was produced at high negative angles of attack.

INTRODUCTION

One of the requirements for supersonic military aircraft is provision for a safe ejection of the crew should the aircraft become disabled. Biomedical studies of the escape phase of air combat missions flown by NATO forces reported in reference 1 have shown a very high injury rate during conventional pilot-parachute ejections. The concept of an escape module which would provide the protection needed during a supersonic ejection, has been studied during the development program of a supersonic military aircraft and as part of this study it was necessary to determine the dynamic-stability characteristics of the

escape module at various attitudes which might be encountered during deployment from the aircraft.

Therefore, longitudinal and lateral dynamic-stability characteristics have been determined for 0.045-scale models of the proposed escape module. Data was obtained in pitch, yaw, and roll at Mach numbers from 0.40 to 1.20 in the Langley 8-foot transonic pressure tunnel and in pitch and yaw at Mach numbers from 1.50 to 2.16 in the Langley Unitary Plan wind tunnel. The tests were made, using a forced oscillation technique, at an oscillation amplitude of about 1° for the tests in pitch and yaw and about 2.5 for the tests in roll. Two models were tested with various offset angles with respect to the support sting in order to provide a wide range of angle of attack. Tests were made to determine the effects of removal of fins, rockets, and spoiler.

The results of these tests, obtained during 1971 and used during the design studies of the proposed escape module, are published herein to provide a contribution to the aerodynamic data base for future studies of similar configurations.

COEFFICIENTS AND SYMBOLS

Measurements were made and are presented herein in the International System of Units (SI). Details concerning the use of SI, together with physical constants and conversion factors, are given in reference 2.

The aerodynamic parameters are referenced to the body-axis systems as shown in figure 1. These axes originate at the center-of-gravity location of the model as shown on figure 2. The equations which were used to reduce the dimensional aerodynamic parameters of the model to nondimensional aerodynamic parameters are presented in the section on "Measurements and Reduction of Data".

f	frequency of oscillation, hertz
k	reduced-frequency parameter $\frac{\omega \ell}{2V}$, radians
ℓ	reference length, 0.142 m
M	free-stream Mach number
p	angular velocity of model about X-axis, rad/s
q	angular velocity of model about Y-axis, rad/s
q_∞	free-stream dynamic pressure N/m^2
R	Reynolds number based on ℓ
r	angular velocity of model about Z-axis, rad/s
S	reference area of model, .0113 m^2
V	free-stream velocity, m/s
C_ℓ	rolling-moment coefficient, $\frac{\text{Rolling moment}}{q_\infty S \ell}$
C_{ℓ_p}	$\frac{\partial C_\ell}{\partial\left(\frac{p\ell}{2V}\right)}$ per radian
$C_{\ell_{\dot{\beta}}}$	$\frac{\partial C_\ell}{\partial\left(\frac{\dot{\beta}\ell}{2V}\right)}$ per radian

$C_{\ell_p} + C_{\ell_{\dot{\beta}}} \sin\alpha$ damping-in-roll parameter, per radian

$C_{\ell_\beta} \sin\alpha - k^2 C_{\ell_{\dot{p}}}$ effective-dihedral parameter

C_m pitching-moment coefficient, $\frac{\text{Pitching moment}}{q_\infty S\ell}$

C_{m_q} $\frac{\partial C_m}{\partial\left(\frac{q\ell}{2V}\right)}$ per radian

$C_{m_{\dot{q}}}$ $\frac{\partial C_m}{\partial\left(\frac{\dot{q}\ell}{4V^2}\right)}$ per radian

$C_{m_q} + C_{m_{\dot{\alpha}}}$ damping-in-pitch parameter, per radian

C_{m_α} $\frac{\partial C_m}{\partial\alpha}$ per radian

$C_{m_{\dot{\alpha}}}$ $\frac{\partial C_m}{\partial\left(\frac{\dot{\alpha}\ell}{2V}\right)}$ per radian

$C_{m_\alpha} - k^2 C_{m_{\dot{q}}}$ oscillatory-longitudinal-stability parameter, per radian

C_n yawing-moment coefficient, $\frac{\text{Yawing moment}}{q_\infty S\ell}$

C_{n_r} $\frac{\partial C_n}{\partial\left(\frac{r\ell}{2V}\right)}$ per radian

$C_{n_{\dot{r}}}$	$\dfrac{\partial C_n}{\partial\left(\dfrac{\dot{r}\ell^2}{4V^2}\right)}$ per radian
$C_{n_r} - C_{n_{\dot{\beta}}} \cos\alpha$	damping-in yaw parameter, per radian
C_{n_β}	$\dfrac{\partial C_n}{\partial \beta}$ per radian
$C_{n_{\dot{\beta}}}$	$\dfrac{\partial C_n}{\partial\left(\dfrac{\dot{\beta}\ell}{2V}\right)}$ per radian
$C_{n_\beta} \cos\alpha + k^2 C_{n_{\dot{r}}}$	oscillatory-directional-stability parameter, per radian
α	angle of attack, degrees or radians or mean angle of attack, degrees
β	angle of sideslip, radians
ω	angular velocity, $2\pi f$, rad/s

A dot over a quantity indicates a first derivative with respect to time. The expressions $\cos\alpha$ and $\sin\alpha$ appear in the lateral parameters since these parameters are referred to the body system of axes.

MODELS AND APPARATUS

Models

The geometric characteristics of the 0.045-scale model of the proposed escape module are presented in figure 2. In order to allow for a large angle-of-attack range without encountering excessive support interference effects, the models were designed to allow the sting entry angle to be changed so as to keep the sting in the model wake throughout the angle-of-attack range. A photograph of one of the models mounted on the oscillatory roll mechanism is shown in figure 3.

The models were machined from aluminum alloy and were provided with removable tails, leading-edge spoilers, and separation rockets. Plates were provided to cover unused sting-entry cavities. A 0.32 cm wide transition strip of number 60 carborundum grit was applied to the leading edge of the model as shown in figure 2a.

Wind Tunnels

Two wind tunnels were used to obtain the data presented herein. Common to both tunnels is the ability to control relative humidity and total temperature of the air in the tunnel in order to minimize the effects of condensation shocks and the ability to vary total pressure in order to vary the test Reynolds number.

The data for Mach numbers from 0.40 to 1.20 were obtained in the Langley 8-foot transonic pressure tunnel. The test section of this single-return wind tunnel is about 2.2 meters square with slotted upper and lower walls to permit continuous operation through the transonic speed range. Test-section Mach numbers from near 0 to 1.30 can be obtained and kept constant by controlling the speed of the tunnel-fan drive motor. The sting-support strut is so designed as to keep the model near the center line of the tunnel through a range of angle of attack from about -3° to about 22° when used in conjunction with the oscillation-balance mechanism that was used for these tests.

The data for Mach numbers of 1.50, 1.80 and 2.16 were obtained in test section number 1 of the Langley Unitary Plan wind tunnel. This single-return tunnel has a test section about 1.2 meters square and about 2.1 meters long. An asymmetric sliding block is used to vary the area ratio in order to vary the Mach number from about 1.47 to 2.87. The angle-of-attack mechanism that was used for these tests has a total range of about 30° when used in conjunction with the oscillation-balance mechansim. A more complete description of the Langley 8-foot transonic pressure tunnel and the Langley Unitary Plan wind tunnel is given in reference 3.

Pitch-Yaw Oscillation-Balance Mechanism

A view of the forward section of the oscillation-balance mechanism which was used for the tests in pitch and yaw is presented in figure 4.

Since the oscillation amplitude is small, the rotary motion of a variable-speed electric motor is used to provide essentially sinusoidal motion to the balance through the crank and crosshead mechanism. The oscillatory motion is about the pivot axis shown in figure 4 which was located at the model station identified as the center of oscillation position in figure 2 except for the high angle of attack position ($60^\circ \leq \alpha \leq 90^\circ$) where the oscillation center was displaced 1.27 cm in the +Z direction from the proposed c.g. location.

The strain-gage bridge which measures the torque required to oscillate the model is located between the model attachment surface and the pivot axis. This torque-bridge location eliminates the effects of pivot friction and the necessity to correct the data for the changing pivot friction associated with changing aerodynamic loads. Although the torque bridge is physically forward of the pivot axis, the electrical center of the bridge is located at the pivot axis so that all torques are measured with respect to the pivot axis.

A mechanical spring, which is an integral part of the fixed balance support, is connected to the oscillation balance at the point of model attachment by means of a flexure plate. After assembly of the oscillation balance and fixed balance support, the flexure plate was electron-beam welded in place in order to minimize mechanical fricition. A strain-gage bridge, fastened to the mechanical spring, provides a signal proportional to the angular displacement of the model with respect to the sting.

Although the forced-oscillation balance may be oscillated through a frequency range from near zero to about 30 hertz, as noted in reference 4,

the most accurate measurements of the damping coefficient are obtained at the frequency of velocity resonance. For these tests, the frequency of oscillation varied from 10 to 17 hertz in pitch and from 12 to 21 hertz in yaw.

Roll Oscillation Balance Mechanism

An oscillating sting-balance system was used to determine the damping-in-roll and effective-dihedral parameters. A 1.5-kW, variable-speed motor was used to oscillate the sting and the model by means of an offset crank to give a sinusoidal motion in roll with an amplitude of 2.5°. Figure 5 shows some details of the roll oscillation sting-balance mechanism. The torsional spring internal to the sting is held fixed to the stationary support sting at one end and is connected to the oscillating outer shaft at the other end by a flexure diaphragm. The torsional spring provides a restoring torque which together with the aerodynamic spring component balances the model inertial forces. The strain-gage balance, which is forward of all the bearings and other friction-producing devices, senses only the aerodynamic forces. A strain-gage bridge, fastened to the torsional spring, provides a signal proportional to the angular displacement of the model with respect to the sting. The oscillatory roll balance mechanism is capable of operating at frequencies from near zero to about 30 hertz. For these tests, the frequency of oscillation varied from 11 to 16 hertz.

MEASUREMENTS AND REDUCTION OF DATA

For the pitching tests, measurements are made of the amplitude of the torque required to oscillate the model in pitch T_Y, the amplitude of the angular displacement in pitch of the model with respect to the sting θ, the phase angle η between T_Y and θ, and the angular velocity of the forced oscillation ω. Some details of the electronic instrumentation used to make these measurements are given in reference 5. The viscous-damping coefficient in pitch C_Y for this single-degree-of-freedom system is computed as

$$C_Y = \frac{T_Y \sin\eta}{\omega \theta}$$

and the spring-inertia parameter in pitch is computed as

$$K_Y - I_Y \omega^2 = \frac{T_Y \cos\eta}{\theta}$$

where K_Y is the torsional-spring coefficient of the system and I_Y the moment of inertia of the system about the body Y-axis.

For these tests, the damping-in-pitch parameter was computed as

$$C_{m_q} + C_{m_{\dot{\alpha}}} = - \frac{2V}{q_\infty S \ell^2} \left[\left(C_Y \right)_{\text{wind on}} - \left(C_Y \right)_{\text{wind off}} \right]$$

and the oscillatory-longitudinal-stability parameter was computed as

$$C_{m_\alpha} - k^2 C_{m_{\dot{q}}} = -\frac{1}{q_\infty S \ell}\left[\left(K_Y - I_Y\omega^2\right)_{\text{wind on}} - \left(K_Y - I_Y\omega^2\right)_{\text{wind off}}\right]$$

Since the wind-off value of C_Y is not a function of oscillation frequency, it is determined at the frequency of wind-off velocity resonance because C_Y can be determined most accurately at this frequency. The wind-off value of $K_Y - I_Y\omega^2$ is determined at the same frequency as the wind-on value of $K_Y - I_Y\omega^2$ since this parameter is a function of frequency.

For the yawing tests, measurements are made of the amplitude of the torque required to oscillate the model in yaw T_Z, the amplitude of the angular displacement in yaw of the model with respect to the sting ψ, the phase angle λ between T_Z and ψ, and the angular velocity of the forced oscillation ω. The viscous-damping coefficient in yaw C_Z for this single-degree-of-freedom system is computed as

$$C_Z = \frac{T_Z \sin\lambda}{\omega\psi}$$

and the spring-inertia parameter in yaw is computed as

$$K_Z - I_Z\omega^2 = \frac{T_Z \cos\lambda}{\psi}$$

where K_Z is the torsional-spring coefficient of the system and I_Z is the moment of inertia of the system about the body Z-axis.

For these tests, the damping-in-yaw parameter was computed as

$$C_{n_r} - C_{n_{\dot{\beta}}} \cos\alpha = - \frac{2V}{q_\infty S \ell^2} \left[\left(C_Z \right)_{\text{wind on}} - \left(C_Z \right)_{\text{wind off}} \right]$$

and the oscillatory-directional-stability parameter was computed as

$$C_{n_\beta} \cos\alpha + k^2 C_{n_{\dot{r}}} = \frac{1}{q_\infty S \ell} \left[\left(K_Z - I_Z \omega^2 \right)_{\text{wind on}} - \left(K_Z - I_Z \omega^2 \right)_{\text{wind off}} \right]$$

The wind-off value of C_Z is determined at the frequency of wind-off velocity resonance and the wind-off and wind-on values of $K_Z - I_Z\omega^2$ are determined at the same frequency.

For the rolling tests, measurements were made of the amplitude of the torque required to oscillate the model in roll T_X, the amplitude of the angular displacement in roll of the model with respect to the fixed portion of the sting ϕ, the phase angle σ between T_X and Φ, and the angular velocity of the forced oscillation ω. The viscous-damping coefficient in roll C_X for this single degree of freedom system was computed as

$$C_X = \frac{T_X \sin\sigma}{\omega \phi}$$

and the spring-inertia parameter in roll was computed as

$$K_X - I_X\omega^2 = \frac{T_X \cos\sigma}{\phi}$$

where K_X is the torsional spring coefficient of the system and I_X is the moment of inertia of the system about the body X-axis.

For these tests, the damping-in-roll parameter was computed as

$$C_{\ell_p} + C_{\ell_\beta} \cdot \sin\alpha = \frac{2V}{q_\infty S \ell^2} \left[\left(C_X\right)_{\text{wind on}} - \left(C_X\right)_{\text{wind off}} \right]$$

and the effective dihedral parameter

$$C_{\ell_\beta} \sin\alpha - k^2 C_{\ell_p} = \frac{1}{q_\infty S \ell} \left[\left(K_X - I_X\omega^2\right)_{\text{wind on}} - \left(K_X - I_X\omega^2\right)_{\text{wind off}} \right]$$

As in the pitch and yaw cases, the wind-off value of C_X is determined at the frequency of wind-off velocity resonance since the value of C_X is independent of frequency and can be determined most accurately at the frequency of velocity resonance. The wind-on and wind-off values of $K_X - I_X\omega^2$ are determined at the same frequency since $K_X - I_X\omega^2$ is a function of frequency.

TESTS AND PRESENTATION OF RESULTS

The dynamic-stability parameters in pitch were measured through a range of mean angle of attack at 0° sideslip with the model oscillating

in pitch about the body Y-axis. To measure the corresponding parameters in yaw, the oscillation balance was rolled 90° within the model to provide oscillation about the body Z axis. The oscillation amplitude for the tests in pitch and yaw was about 1°.

The model was mounted on a separate oscillatory roll balance to obtain the corresponding dynamic-stability parameters in roll. The amplitude of the oscillations in roll was 2.5°.

Test conditions are shown in the following table:

M	T_t, K	q_∞, kN/m^2	R
0.40	322	13.3	1.40×10^6
.80	↓	23.8	↓
.95		26.6	
1.03		27.9	
1.20		30.0	
1.50	328	32.8	
1.80	↓	33.0	
2.16		31.9	

The reduced-frequency parameter varied from 0.0103 to 0.0650 for the tests in pitch and yaw and from 0.0139 to 0.0494 for the tests in roll. In addition to testing the complete configuration, tests also were made to determine the effects of various model components.

An index to the figures used to present the results of this investigation is as follows:

	Figure
Longitudinal-Stability Characteristics	
Basic model	6
Fins off	7
Effect of component buildup	8
Lateral-Stability Characteristics	
Basic model, yaw	9
Basic model, roll	10

Positive damping and stability in pitch are indicated by negative values of $C_{m_q} + C_{m_{\dot{\alpha}}}$ and $C_{m_\alpha} - k^2 C_{m_{\dot{q}}}$. Positive damping in yaw is indicated by negative values of $C_{n_r} - C_{n_{\dot{\beta}}} \cos\alpha$ while positive oscillatory stability in yaw is indicated by positive values of $C_{n_\beta} \cos\alpha + k^2 C_{n_{\dot{r}}}$. Positive damping in roll is indicated by negative values of $C_{\ell_p} + C_{\ell_{\dot{\beta}}} \sin\alpha$. Positive effective dihedral is indicated by negative values of $C_{\ell_\beta} \sin\alpha - k^2 C_{\ell_{\dot{p}}}$.

Sketches have been included at the top of the data figures which show the model-sting orientation used to obtain the various segments of the angle-of-attack range. As noted on the sketches, for the extreme angle-of-attack ranges the rocket nozzles were not used even for the so-called basic configuration due to certain mechanical constraints imposed by these particular model-sting orientations. Since the nozzles, had they

been present, would have been completely submerged in the forebody wake for the lowest angle-of-attack range, it is believed that the data taken without the nozzles is a fair representation of the data which one would obtain for the complete configuration. However, in the highest angle-of-attack range, the presence or absence of the nozzles would perhaps be expected to have an appreciable influence on the aerodynamic data. No analysis has been made to determine the magnitude of any effect on the data due to the absence of the nozzles. The data obtained in the highest angle-of-attack range should be used with discression, keeping in mind that the presence or absence of the nozzles may have a significant influence on the aerodynamic data.

DISCUSSION OF RESULTS

Damping and Oscillatory Stability in Pitch

Figures 6 through 8 present the damping-in-pitch parameter $C_{m_q} + C_{m_{\dot{\alpha}}}$ and the oscillatory-longitudinal-stability parameter $C_{m_\alpha} - k^2 C_{m_{\dot{q}}}$. Component build-up data were taken from some portions of the angle-of-attack and Mach number ranges. In the negative and low positive angle of attack range the configuration, in general, exhibited positive damping. However in the moderate and high positive angle of attack range some negative damping is observed. Although the fin-off data (fig 7) is rather limited in angle-of-attack range it does indicate that the initial negative damping region is associated with a negative damping contribution from

the fins. It would appear that the high positive and negative excursions in the aerodynamic characteristics may be caused by vortex flow over the fins and/or by fin stall.

Damping and Oscillatory Stability in Yaw

The damping-in-yaw parameter $C_{n_r} - C_{n_{\dot{\beta}}} \cos\alpha$ and the oscillatory-directional-stability parameter $C_{n_\beta} \cos\alpha + k^2 C_{n_{\dot{r}}}$ are shown in figure 9. No component build-up tests were made in yaw. There were no pronounced variations of damping in yaw with angle of attack over the Mach range investigated. The oscillatory stability in yaw appears to be varying from unstable to stable in going from negative α to positive α with this effect diminishing with increase in Mach number.

Damping and Oscillatory Stability in Roll

The damping-in-roll parameter $C_{\ell_p} + C_{\ell_{\dot{\beta}}} \sin\alpha$ and the effective-dihedral parameter $C_{\ell_\beta} \sin\alpha - k^2 C_{\ell_{\dot{p}}}$ are shown in figure 10. No unusual excursions were seen in these areas. Except for the highest Mach number, negative damping in roll was produced at high negative α values.

CONCLUDING REMARKS

Wind-tunnel measurements of the aerodynamic damping and oscillatory stability of a model of a proposed escape module for a military aircraft have been made in pitch and yaw at Mach numbers from 0.40 to 2.16 and in

roll at Mach numbers from 0.40 to 1.20 by using a small-amplitude forced-oscillation technique.

The results in pitch indicate regions in the angle-of-attack range where the model exhibits large and rapid changes in both damping and stability with angle of attack, probably caused by vortex flow over the fins. There was no pronounced effect of change in angle of attack on damping in yaw. Except for the highest Mach number, negative damping in roll was produced at high negative angles of attack.

REFERENCES

1. Jones, W. L.: Escape Problems and Manoeuvres in Combat Aircraft. AGARD-CP-134, (Paper presented at the Aerospace Medical Panel Specialists Meeting held at Soesterberg, Netherlands, 4th Sept. 1973).

2. Mechtly, E. A.: The International System of Units - Physical Constant and Conversion Factors (Second Revision). NASA SP-7012, 1973

3. Schaefer, William T., Jr.: Characteristics of Major Active Wind Tunnels at the Langley Research Center, NASA TM X-1130, 1965.

4. Braslow, Albert L.; Wiley, Harleth G.; and Lee, Cullen Q.: A Rigidly Forced Oscillation System for Measuring Dynamic-Stability Parameters in Transonic and Supersonic Wind Tunnels. NASA TN D-1231, 1962. (Supersedes NACA RM L58A28).

5. Wright, Bruce R.; and Kilgore, Robert A.: Aerodynamic Damping and Oscillatory Stability in Pitch and Yaw of Gemini Configurations at Mach Numbers from 0.50 to 4.63. NASA TN D-3334, 1966.

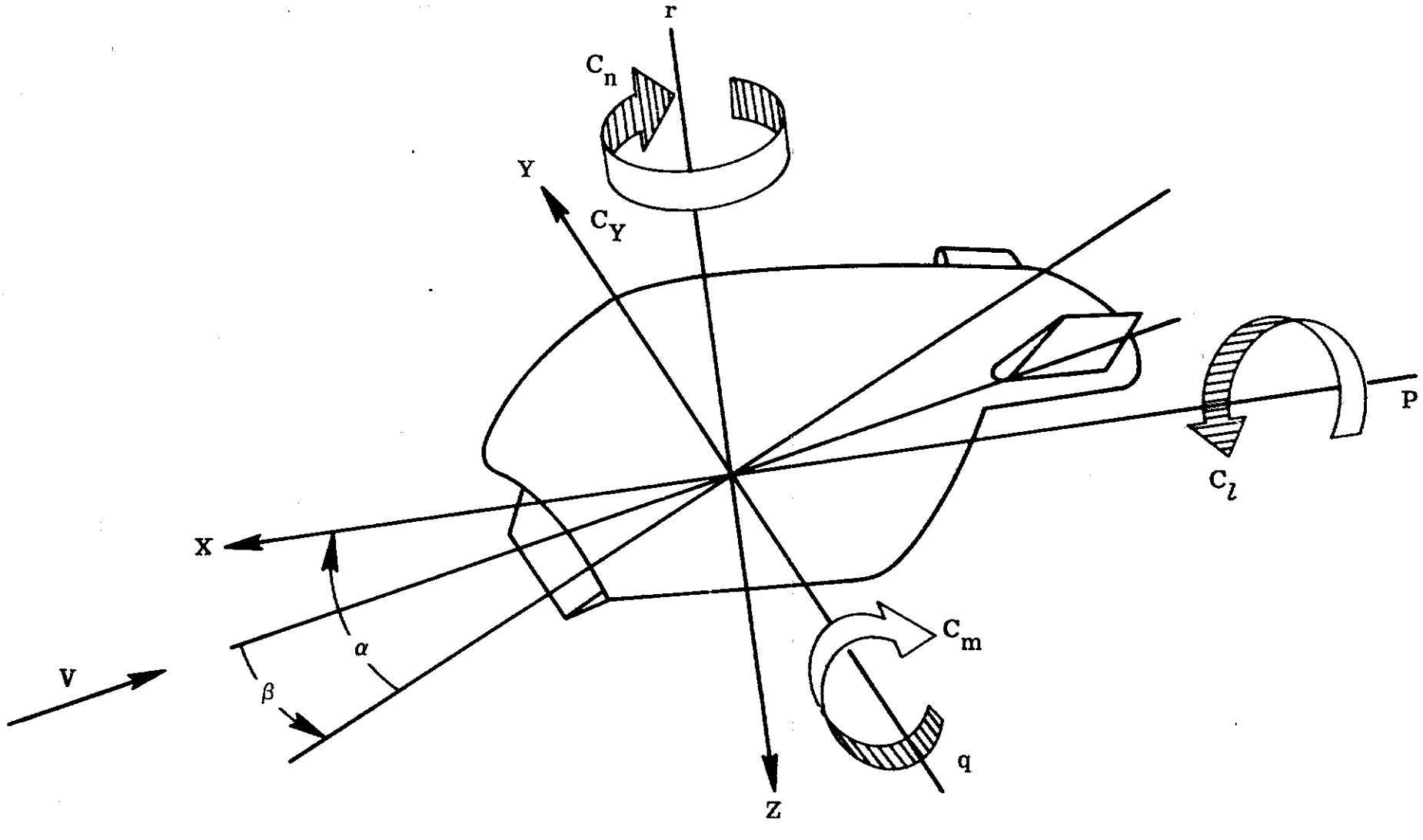

Figure 1.- Body system of axes all angles, anguler velocities, and coefficients shown positive.

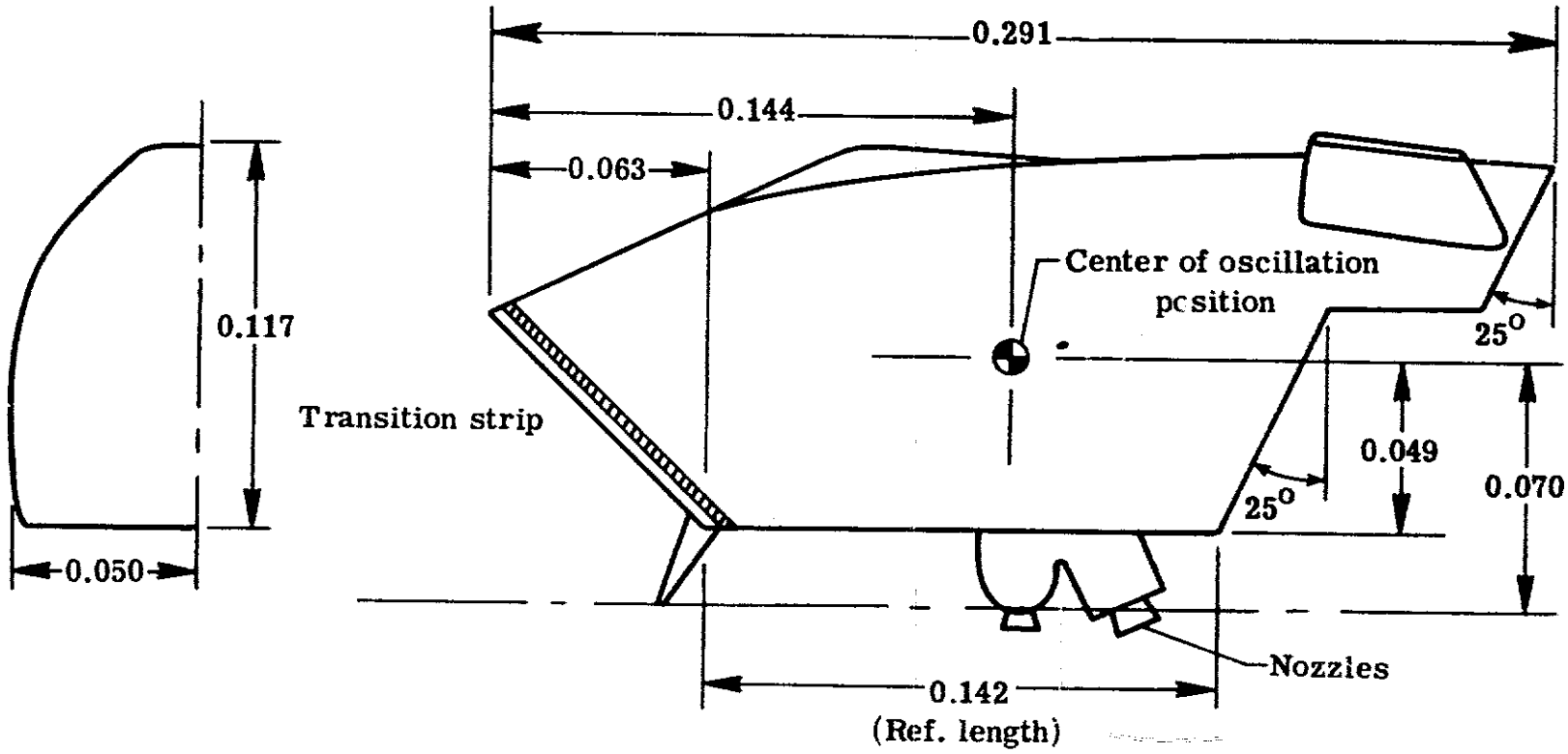

(a) General assembly

Figure 2.- Geometric details of model. (Dimensions are in meters)

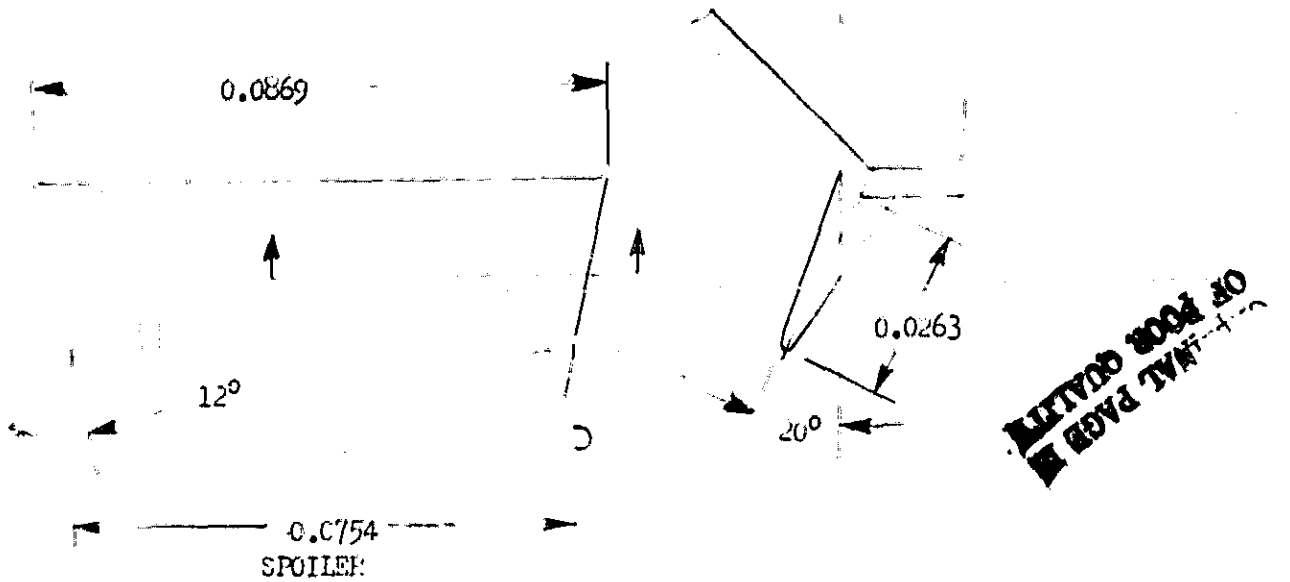

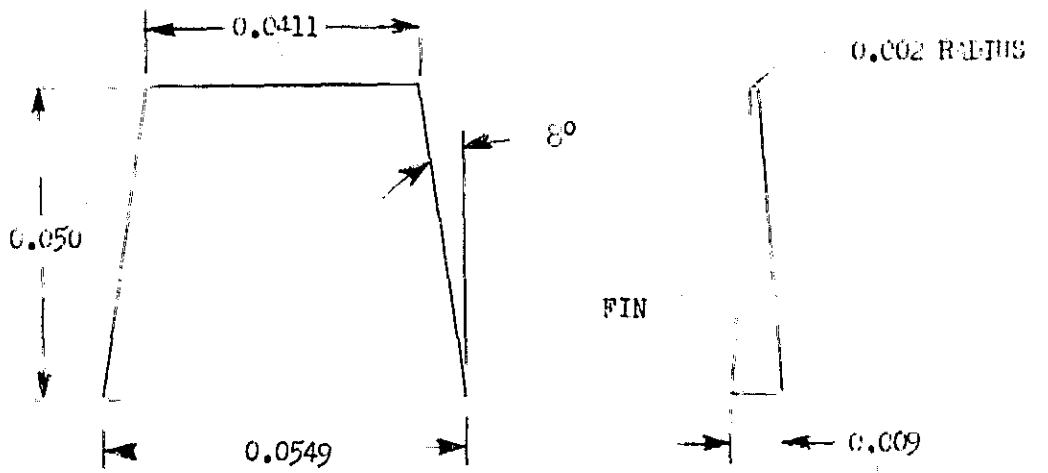

(b) Fin and spoiler details

Figure 2.- Concluded.

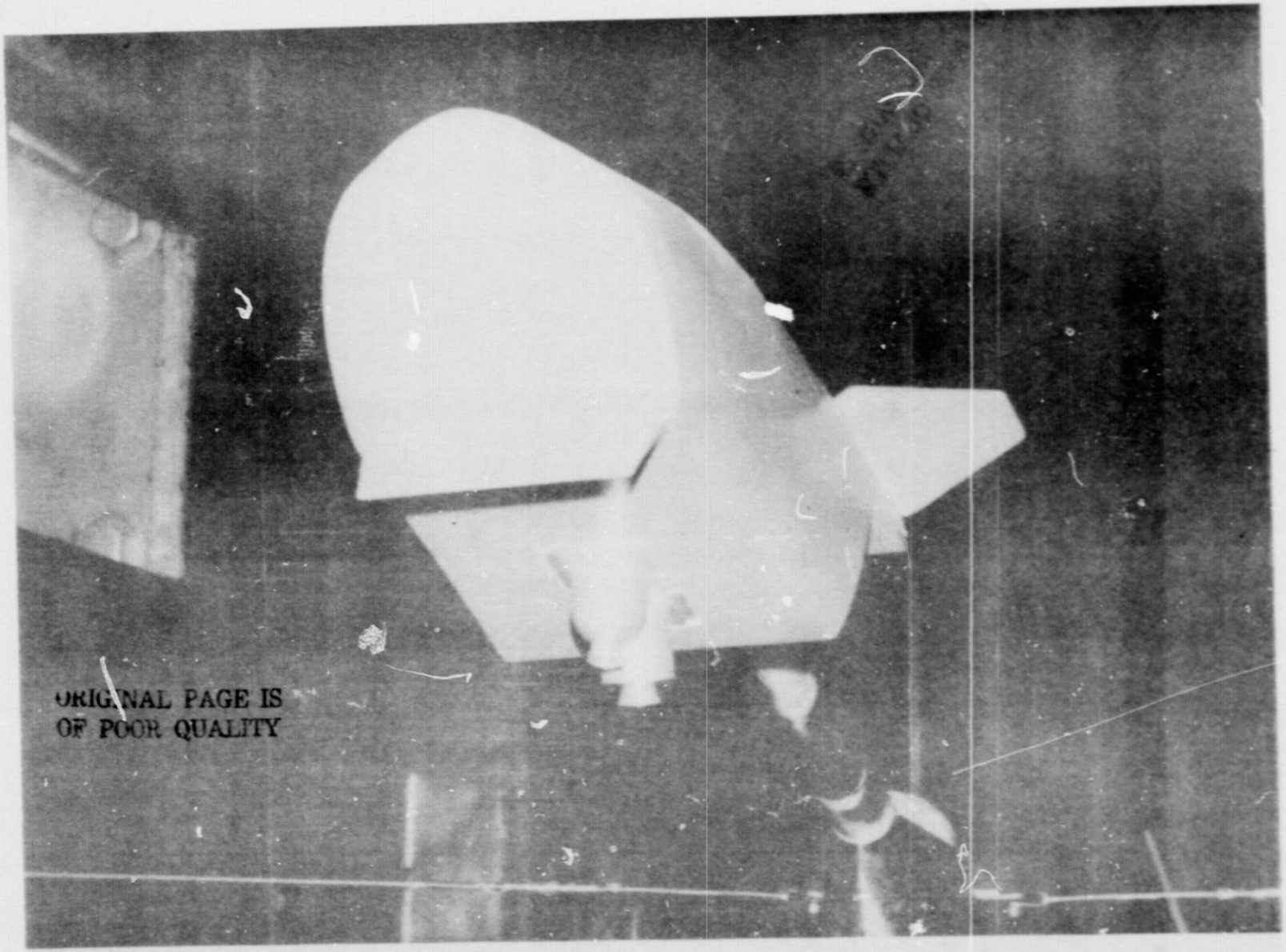

Figure 3.- Photograph of model mounted on the oscillatory roll mechanism in the eight-foot transonic pressure tunnel.

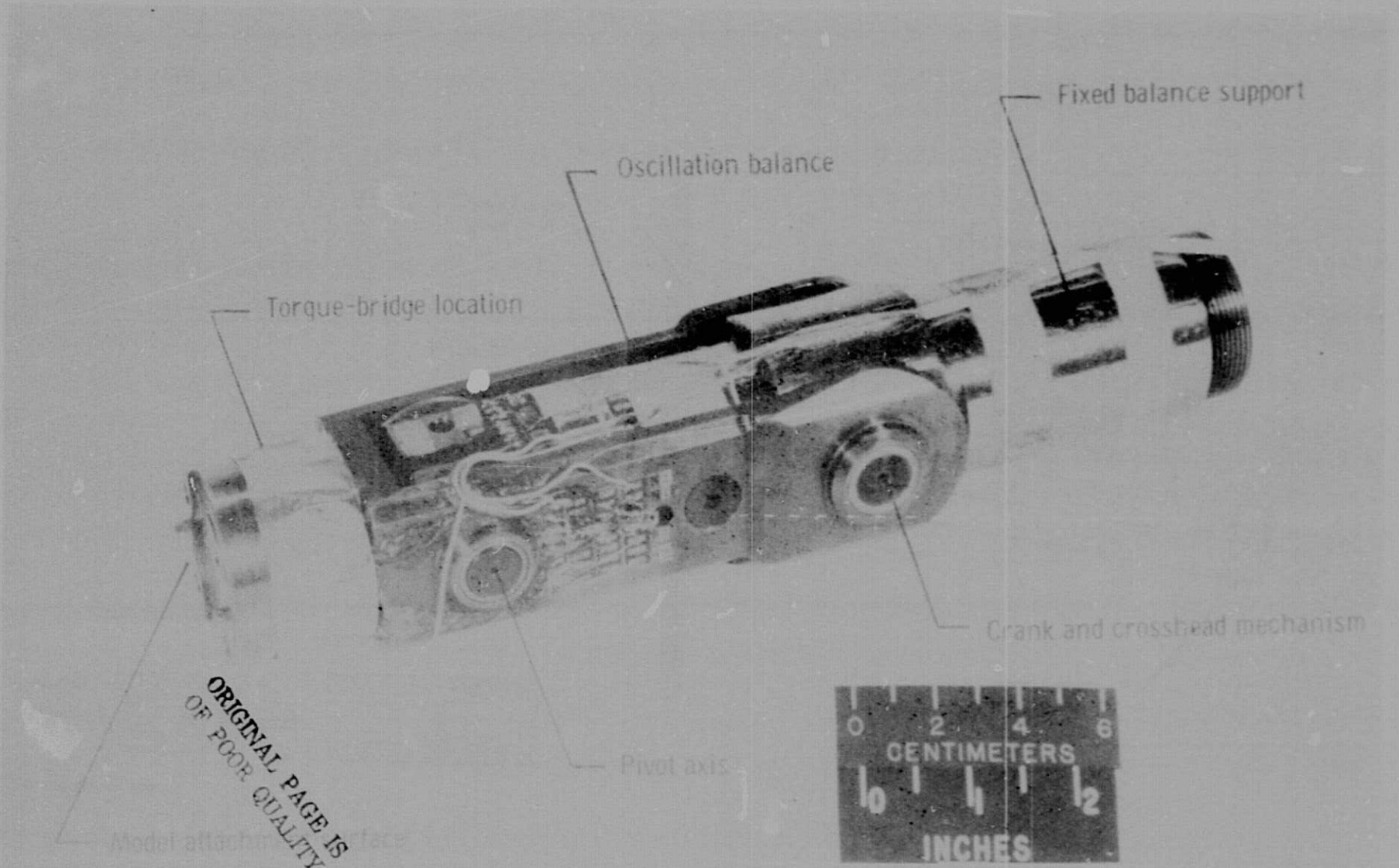

Figure 4.- Forward section of pitch-yaw balance mechanism.

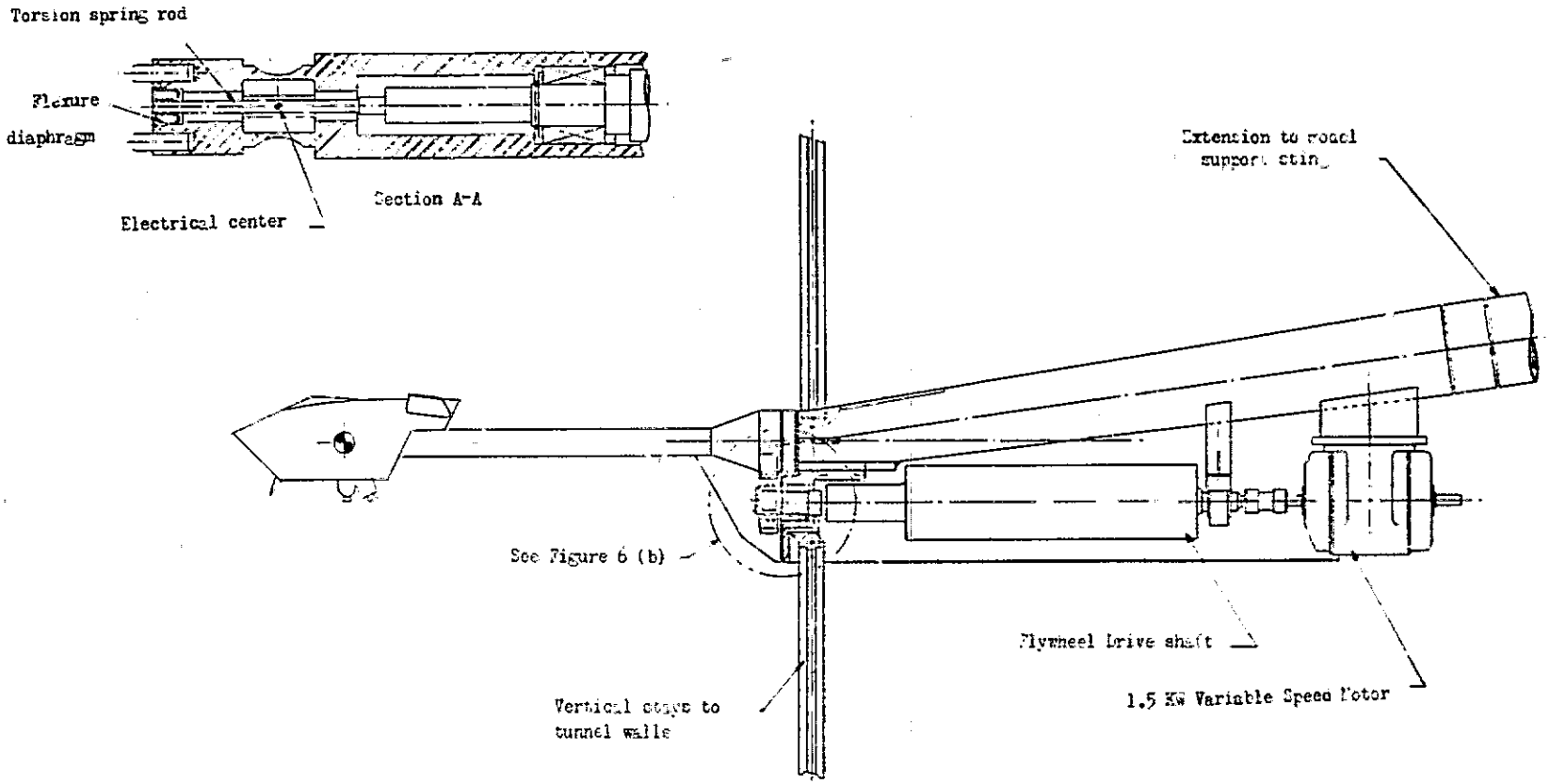

(a) Overall view

Figure 5. - Sketch of roll oscillation balance mechanism with a model.

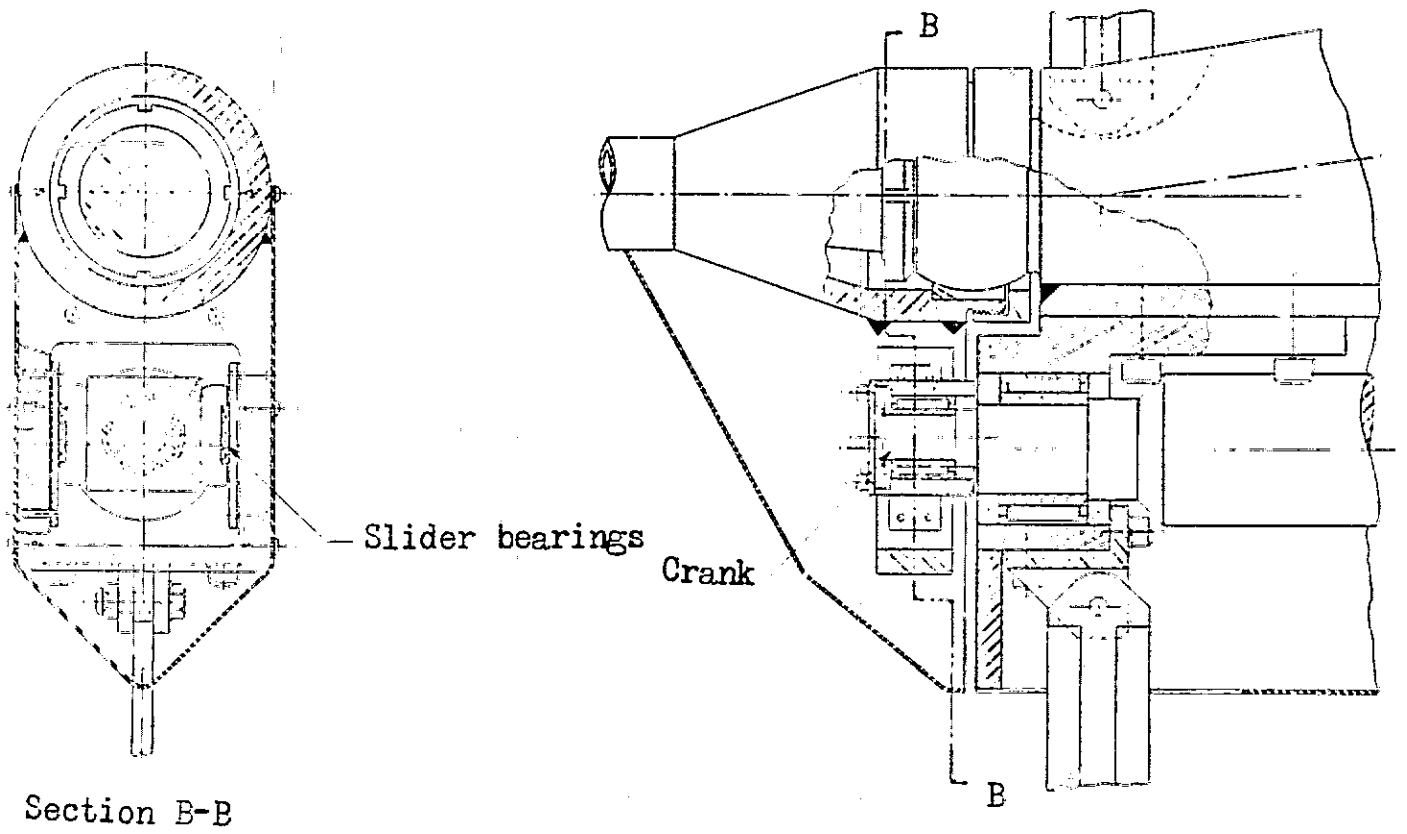

(b) Details

Figure 5.- Concluded.

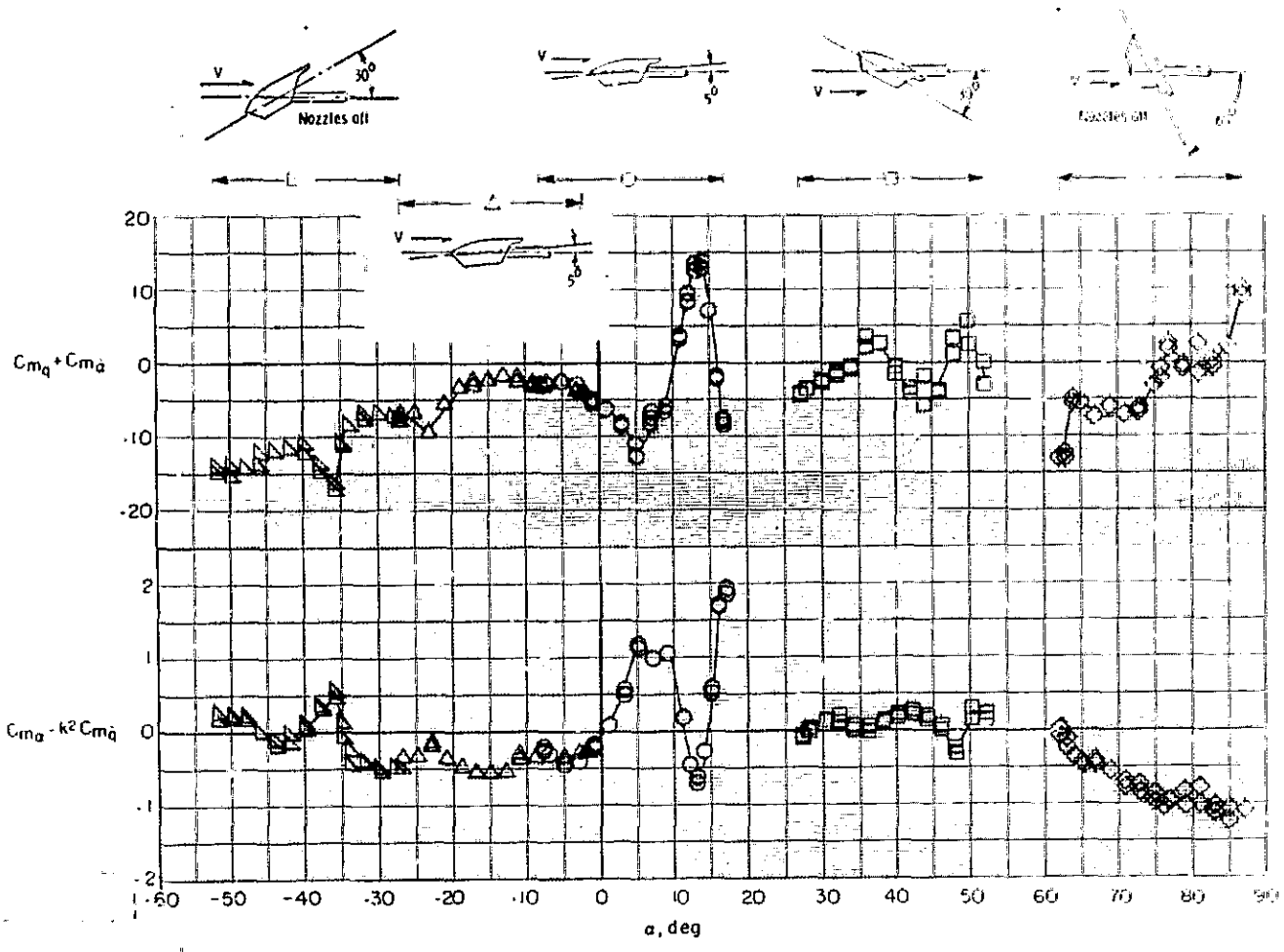

(a) M = 0.4

Figure 6.- Variation of longitudinal dynamic stability characteristics with mean angle of attack. (Nozzles on and off)

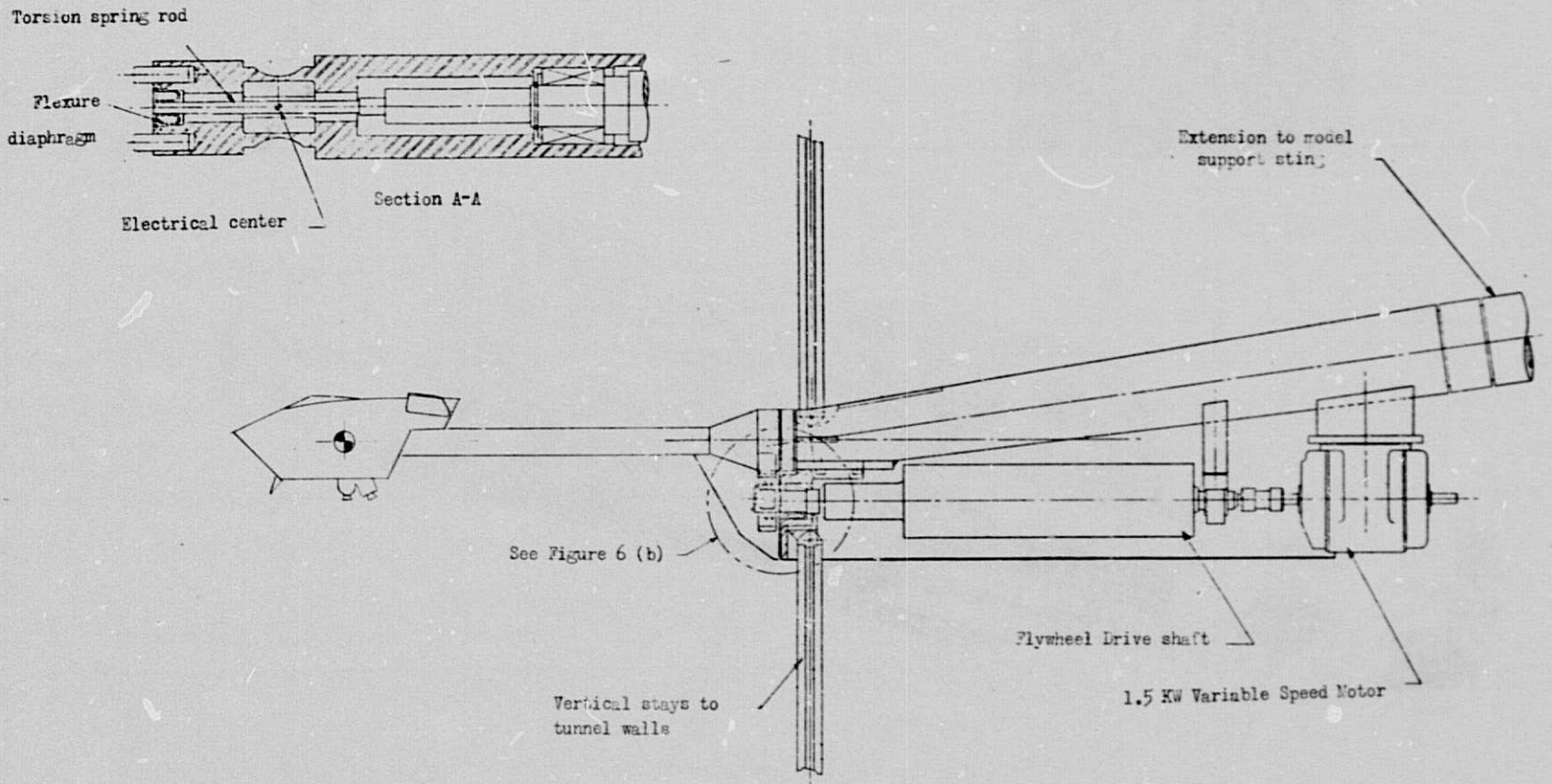

(a) Overall view

Figure 5. - Sketch of roll oscillation balance mechanism with a model.

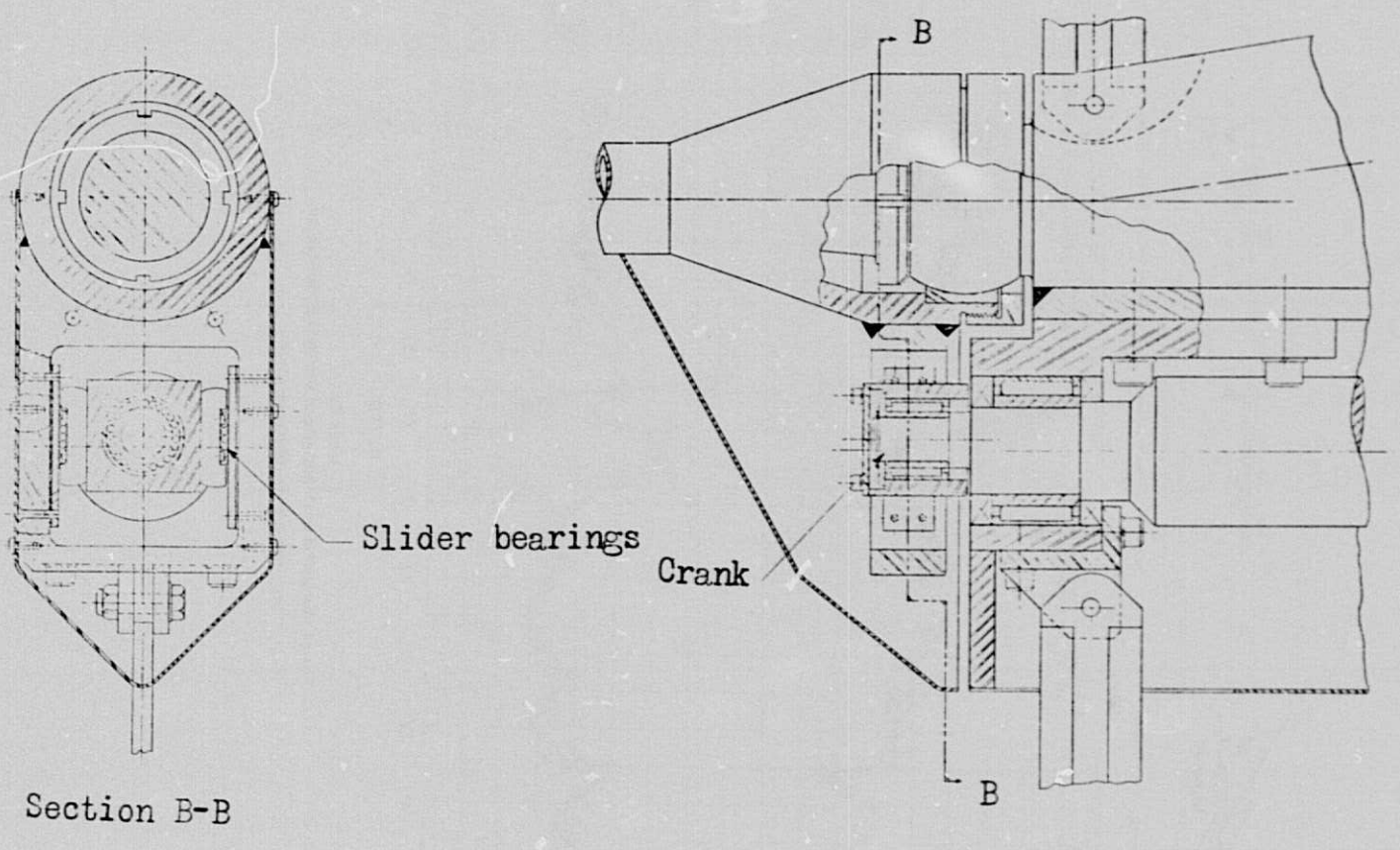

(b) Details

Figure 5.- Concluded.

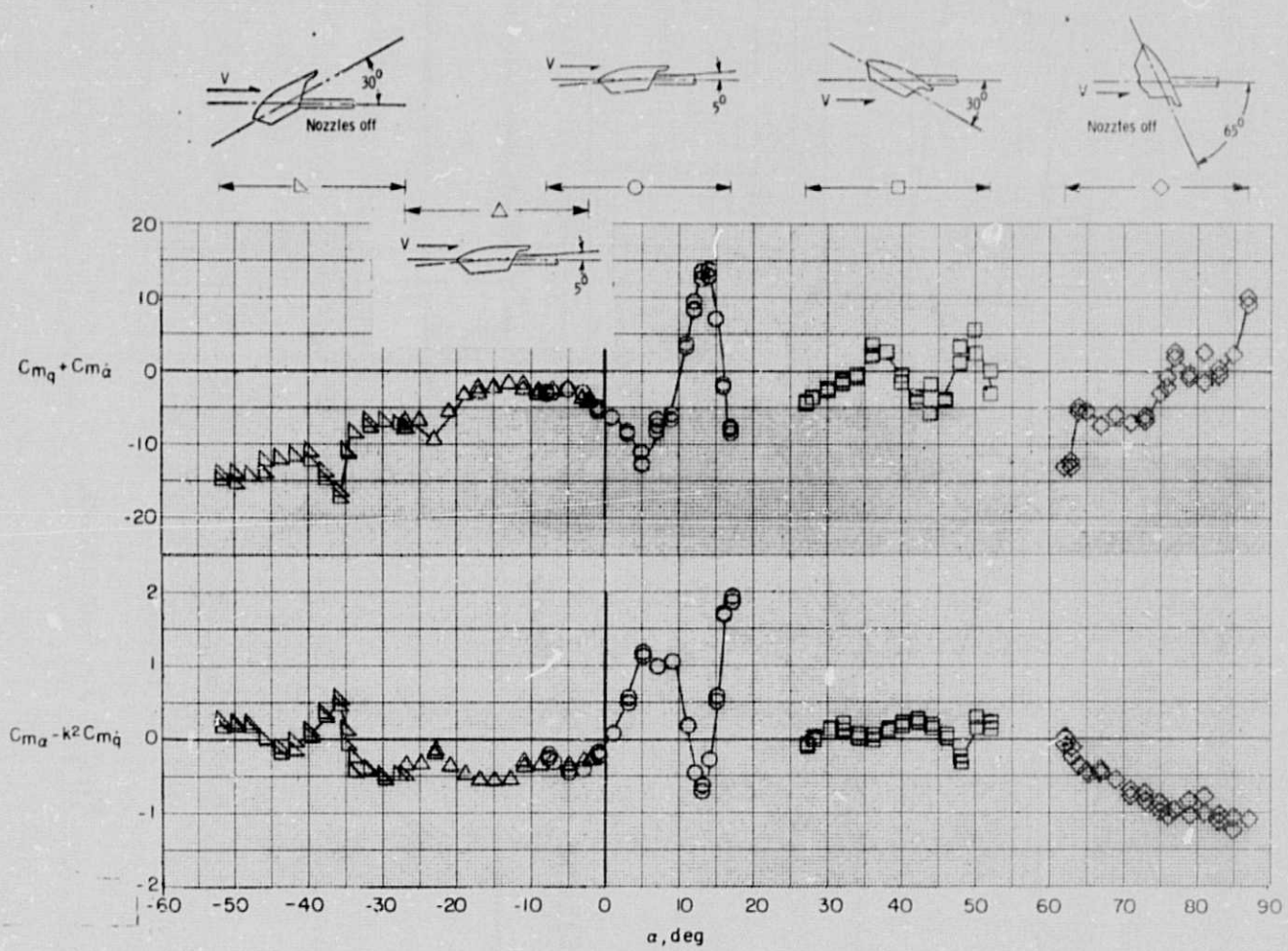

(a) M = 0.4

Figure 6.- Variation of longitudinal dynamic stability characteristics with mean angle of attack. (Nozzles on and off)

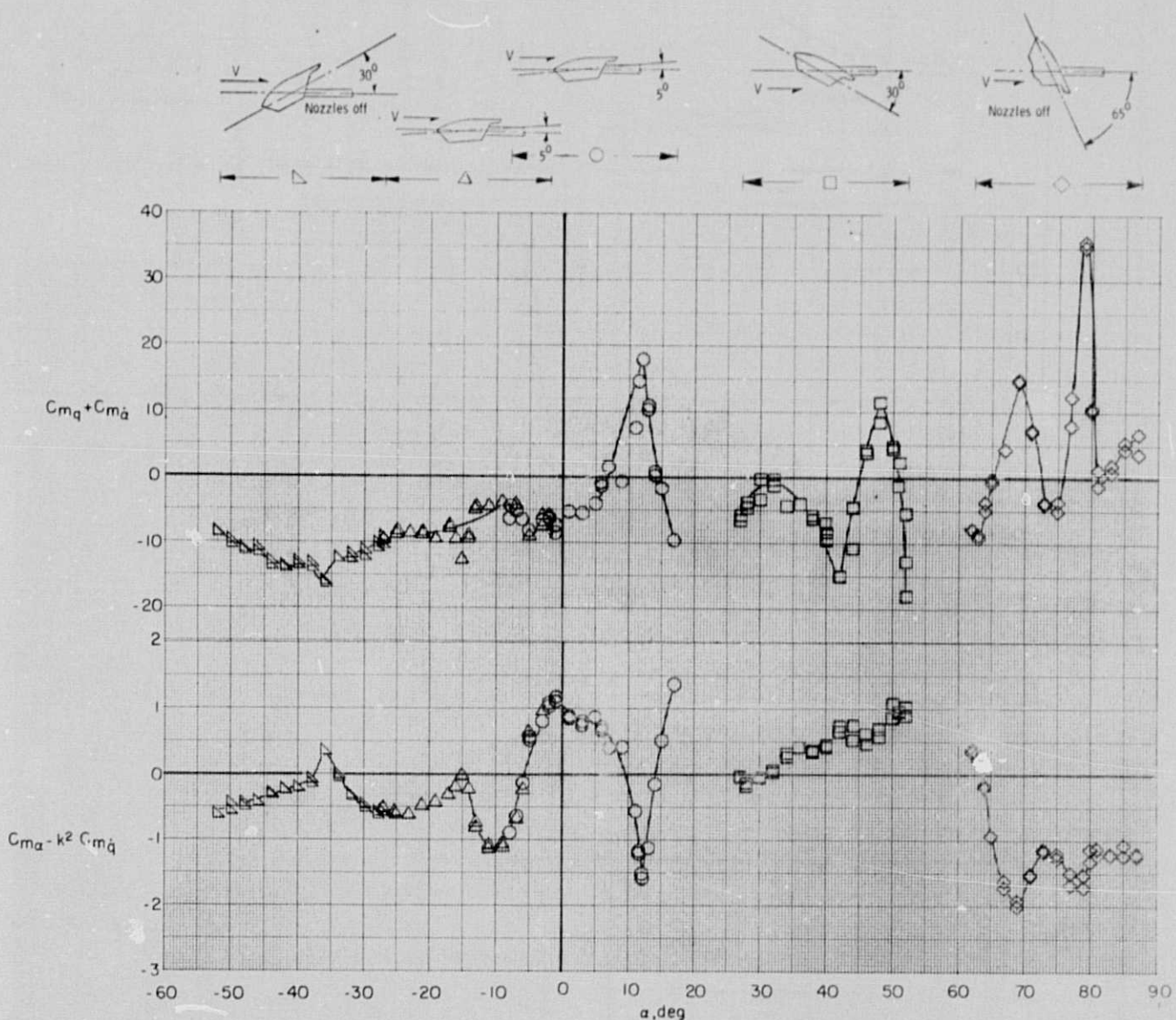

(b) M = 0.8

Figure 6. - Continued.

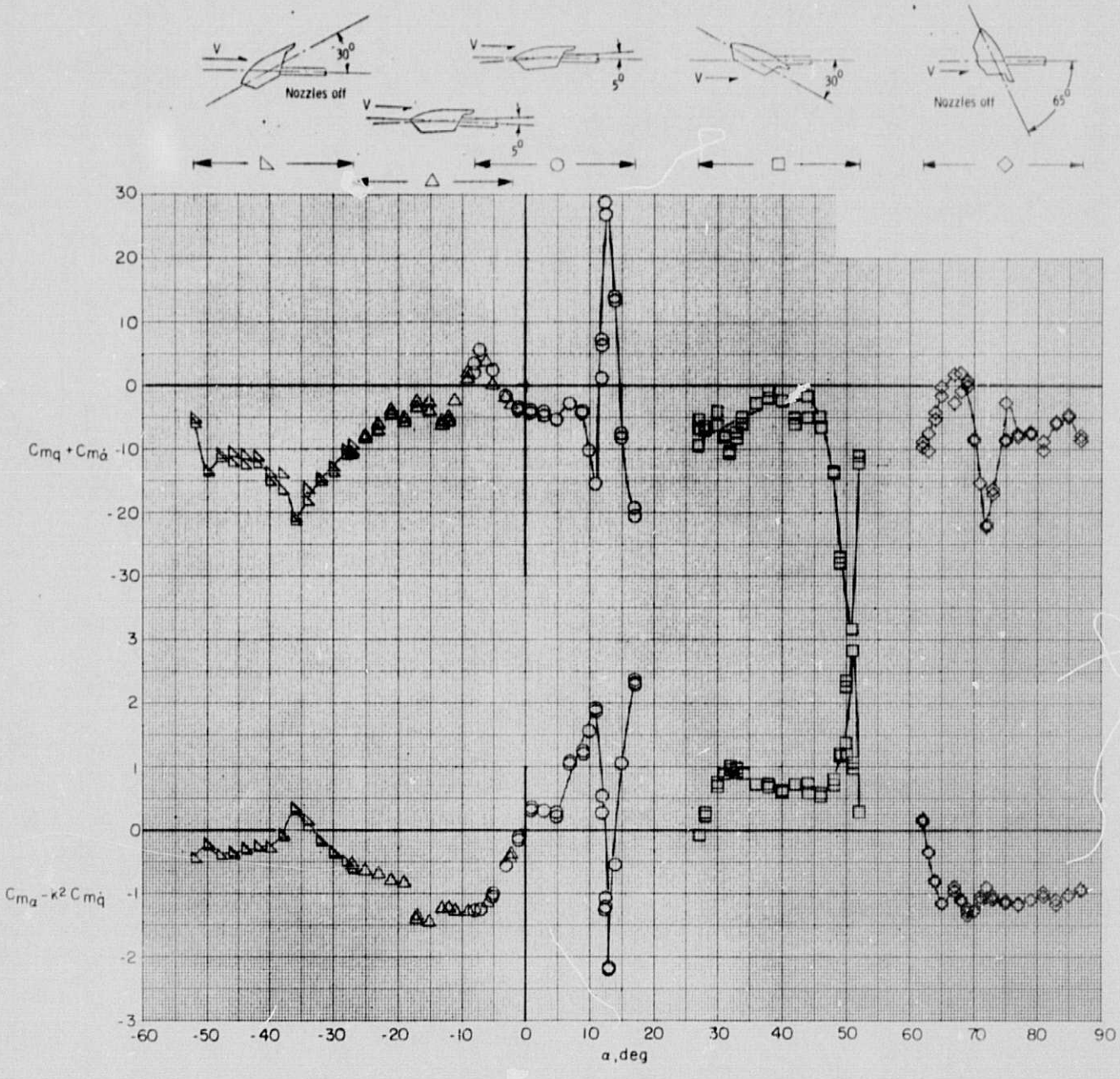

(c) M = 0.95

Figure 6. - Continued.

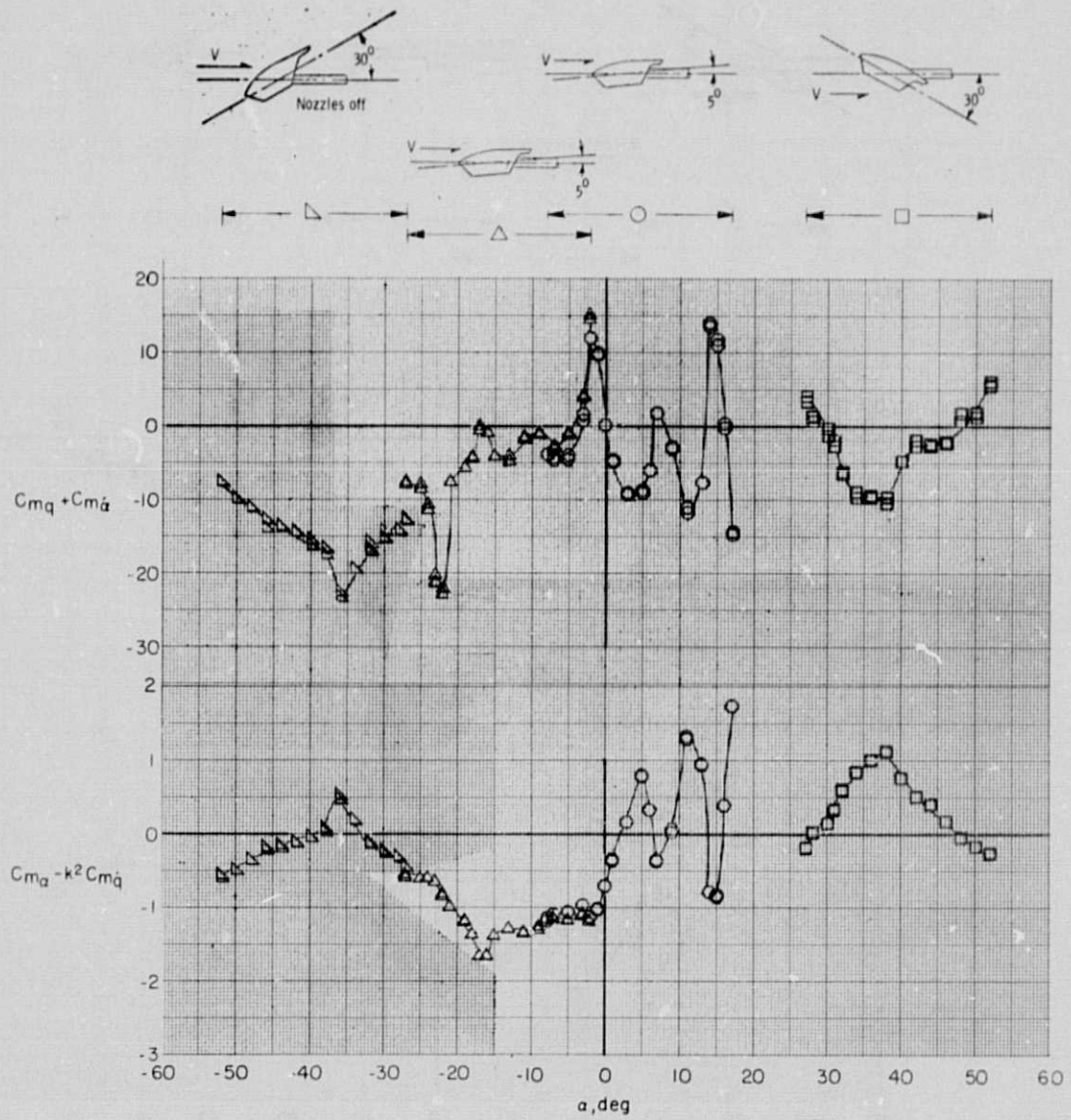

(d) $M_\infty = 1.03$

Figure 6. - Continued.

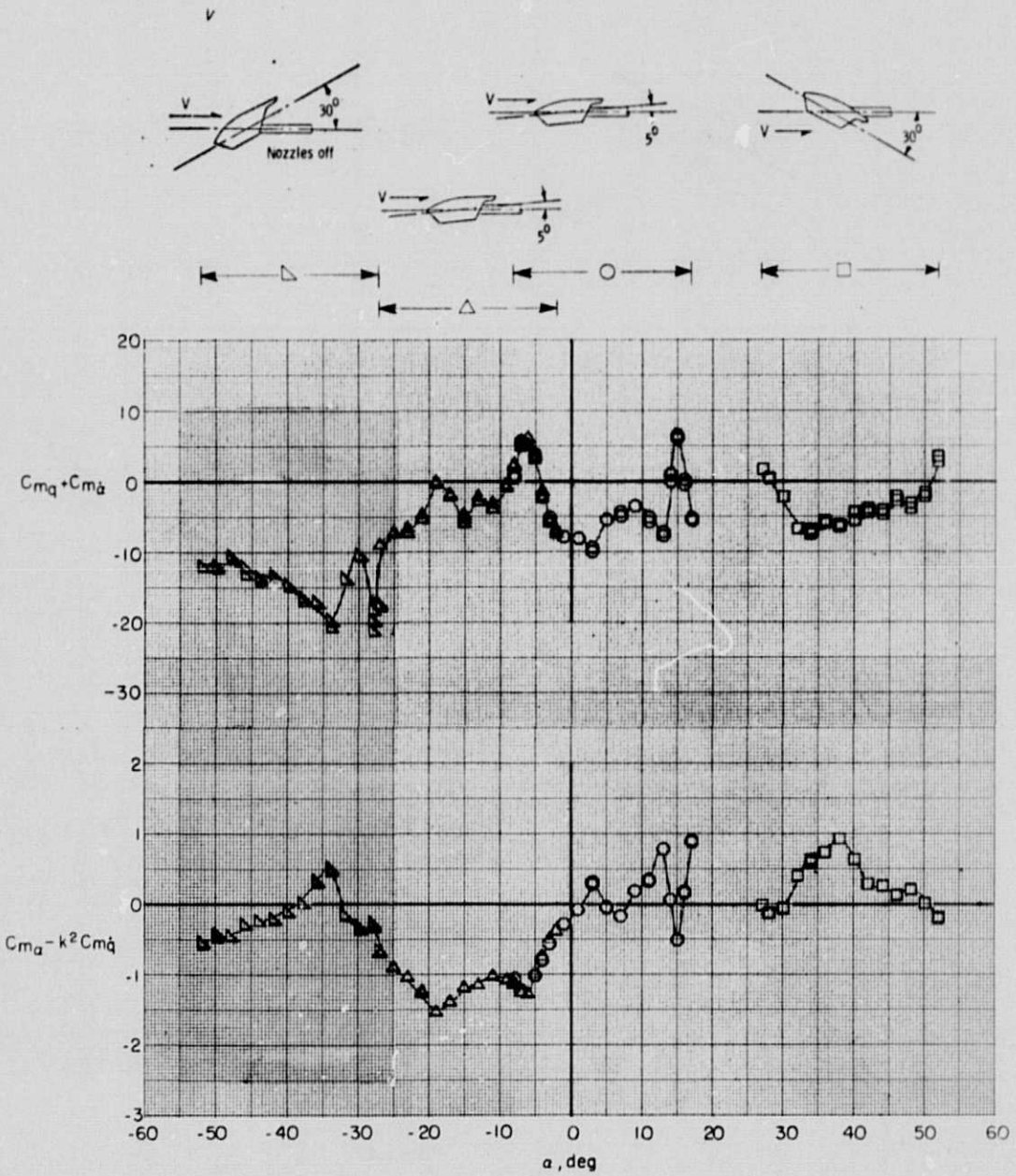

(e) M = 1.2

Figure 6. - Continued.

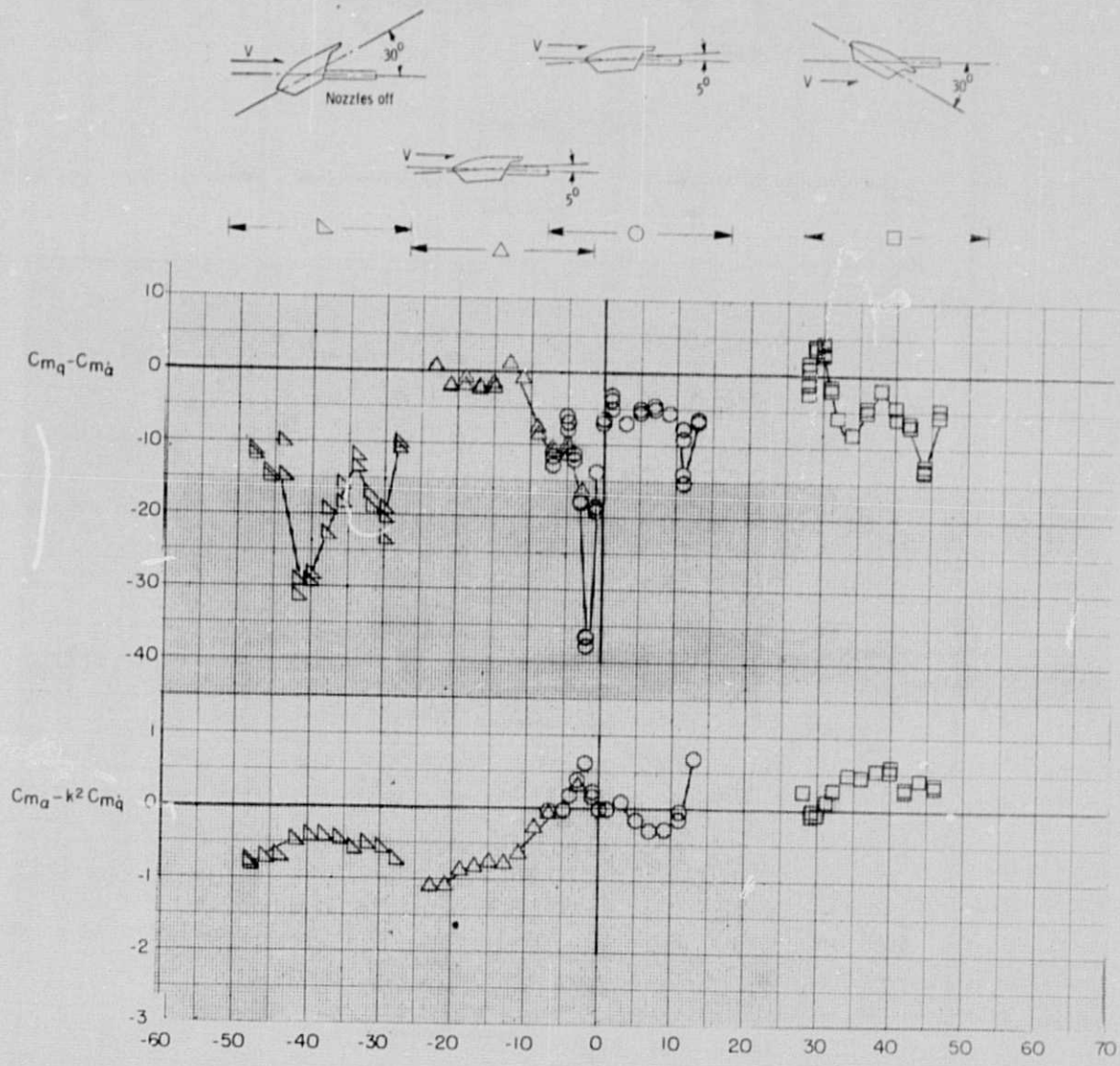

(f) M = 1.5

Figure 6, - Continued.

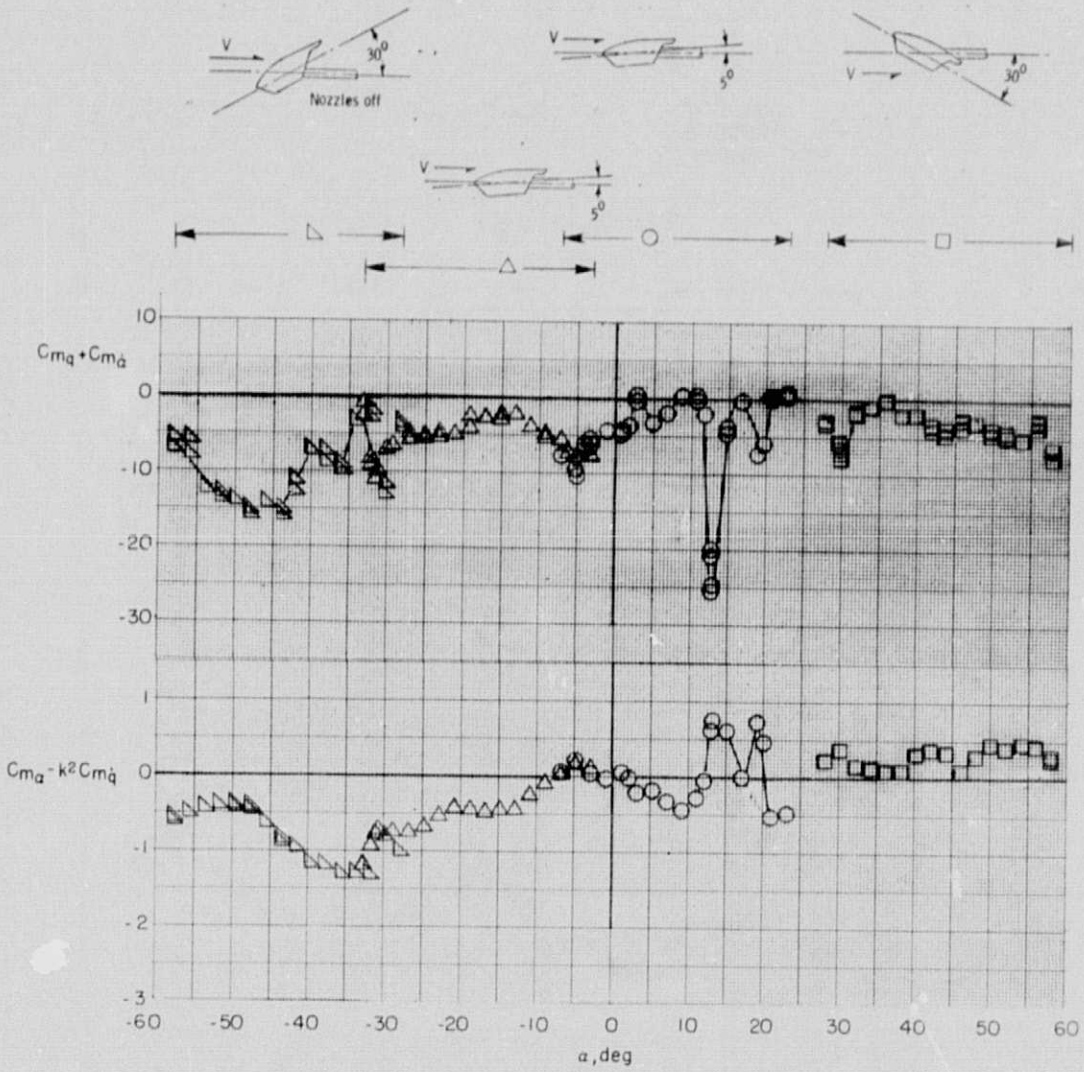

(g) M = 1.8

Figure 6. - Continued.

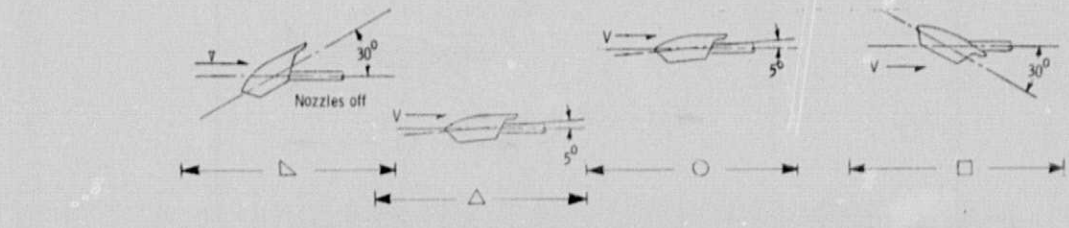

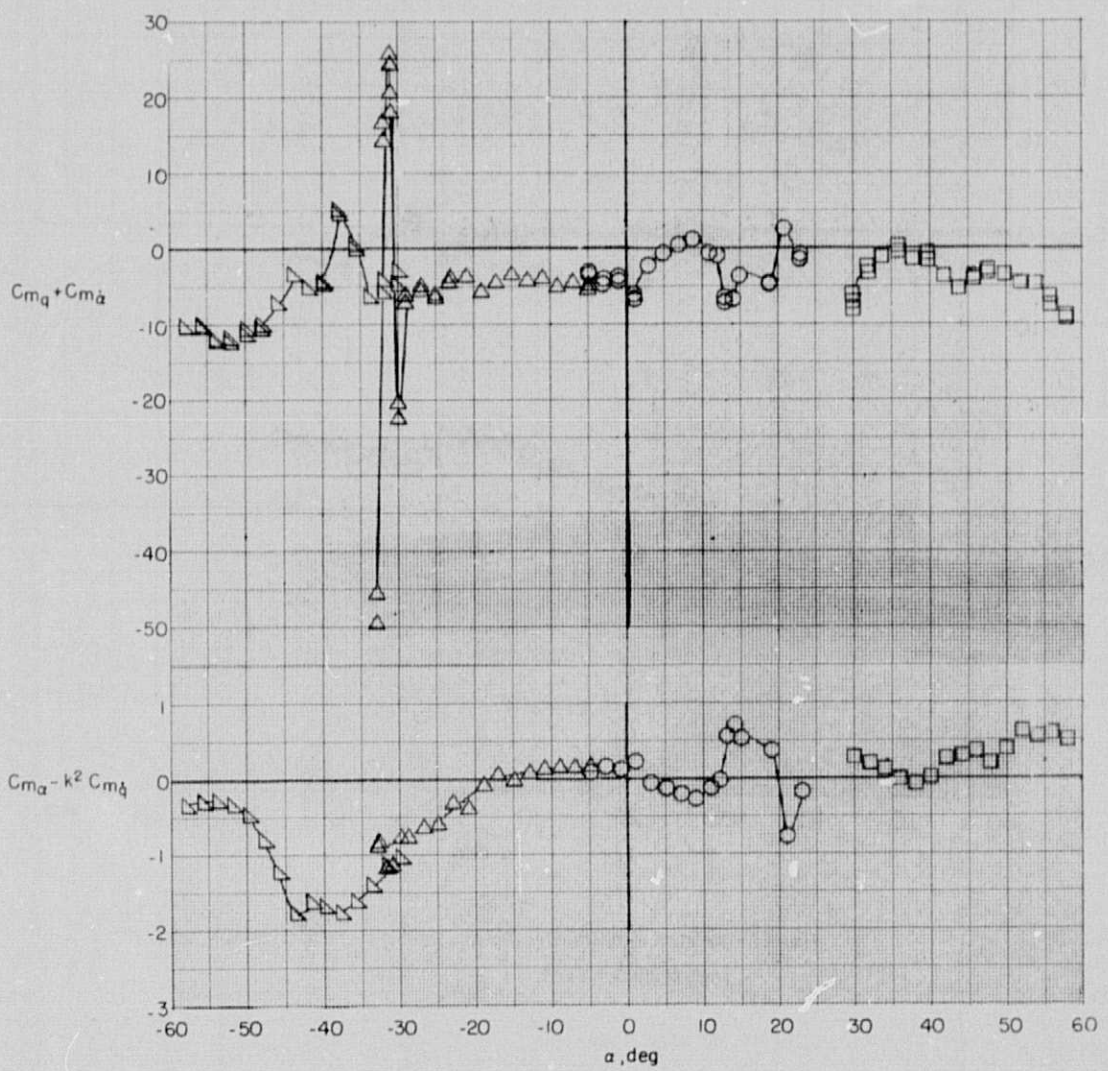

(h) M = 2.16

Figure 6.- Concluded.

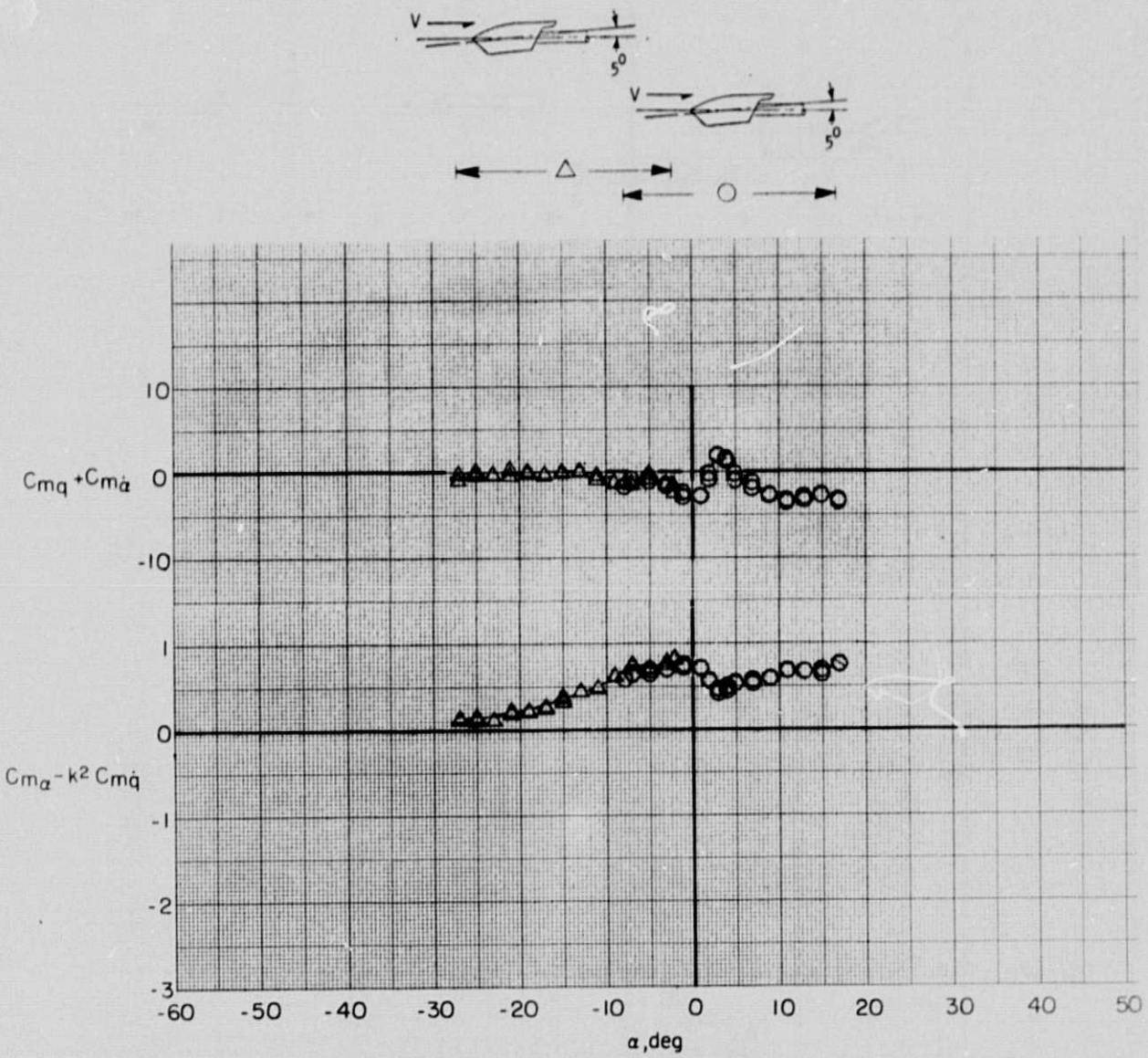

(a) M = 0.4

Figure 7.- Variation of longitudinal dynamic stability characteristics with mean angle of attack, fins off.

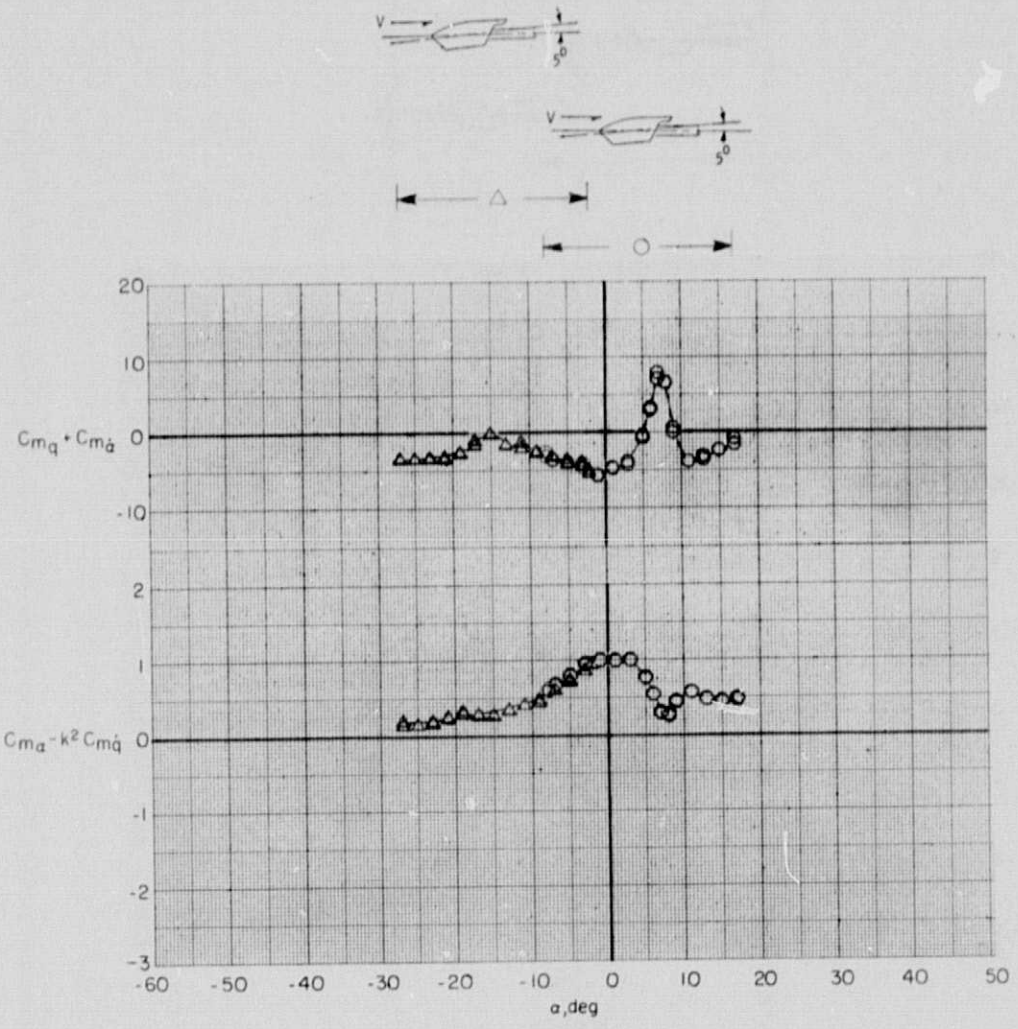

(b) M = 0.8

Figure 7. - Continued.

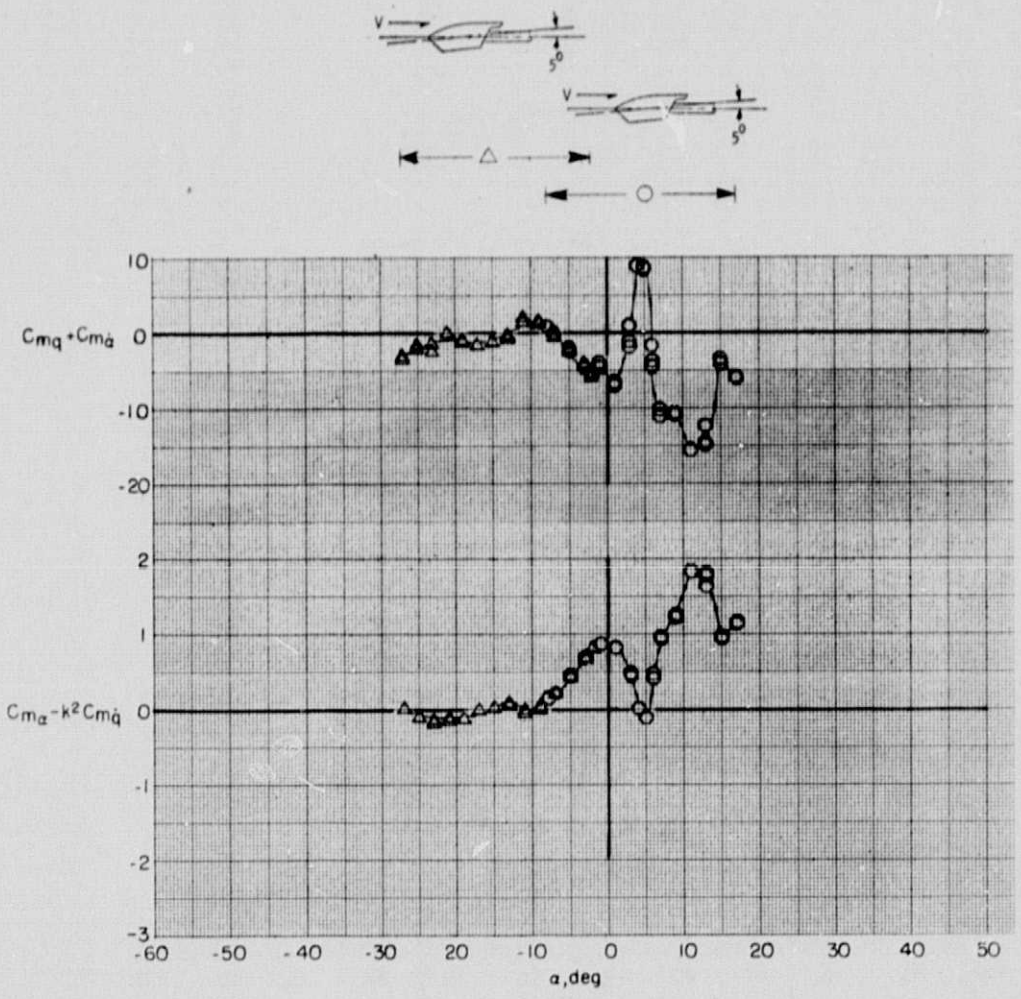

(c) M = 0.95

Figure 7.- Continued.

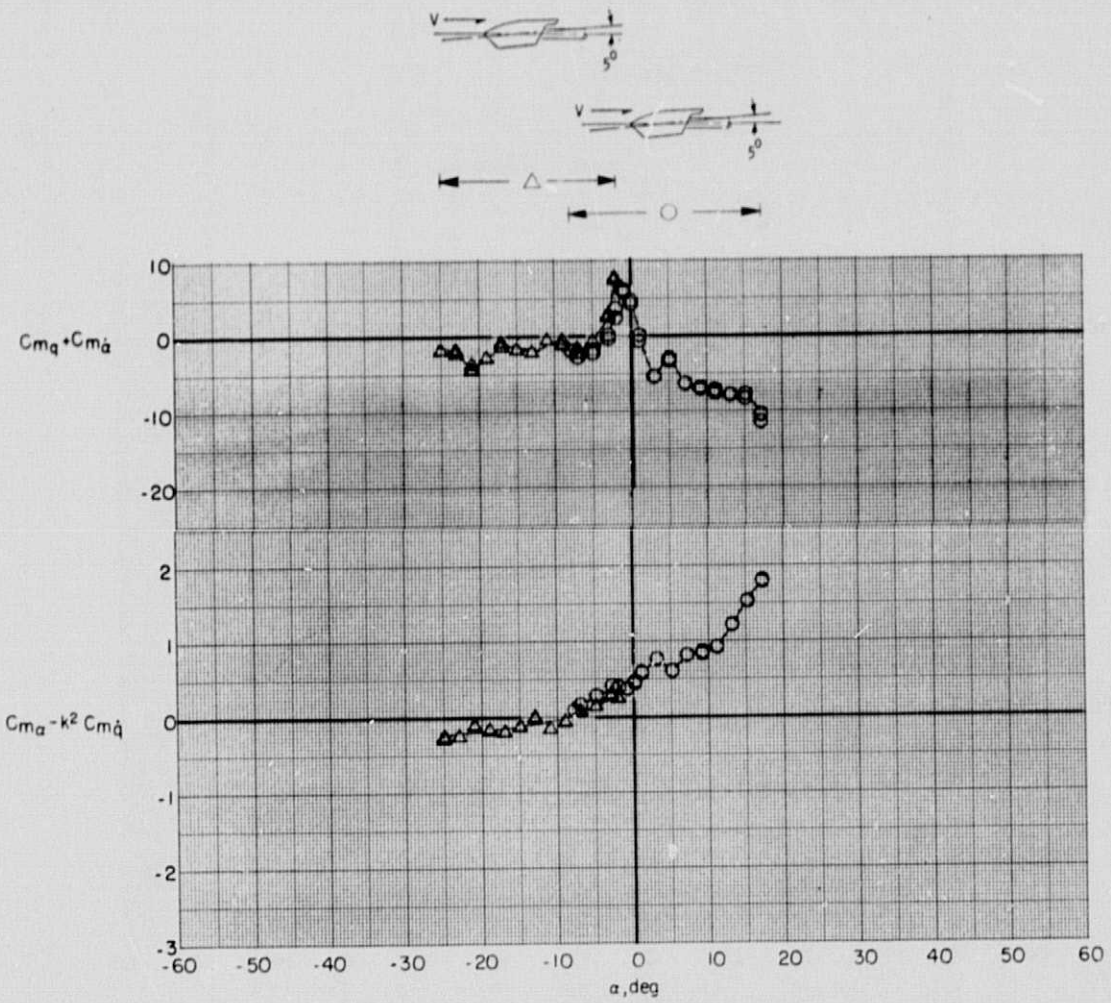

(d) M = 1.03

Figure 7.- Continued.

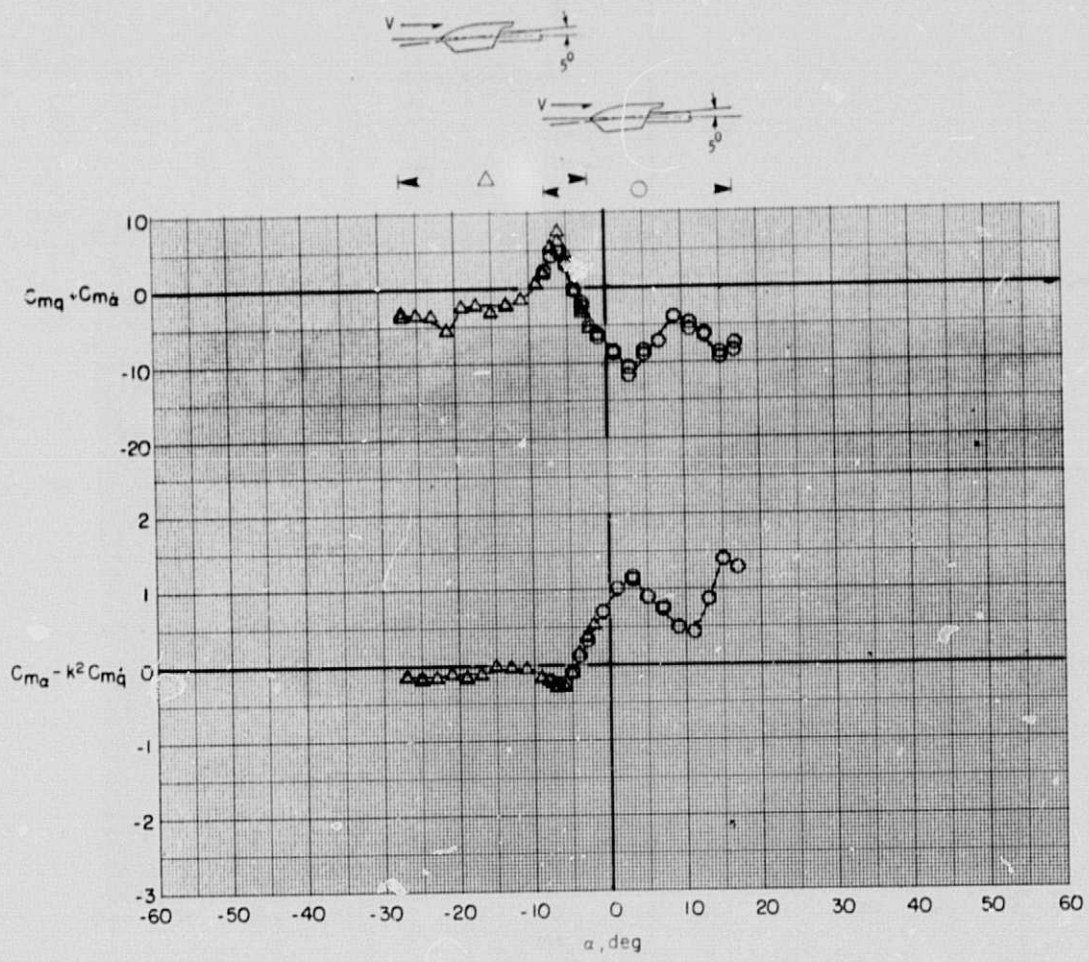

(e) M = 1.2

Figure 7.- Concluded.

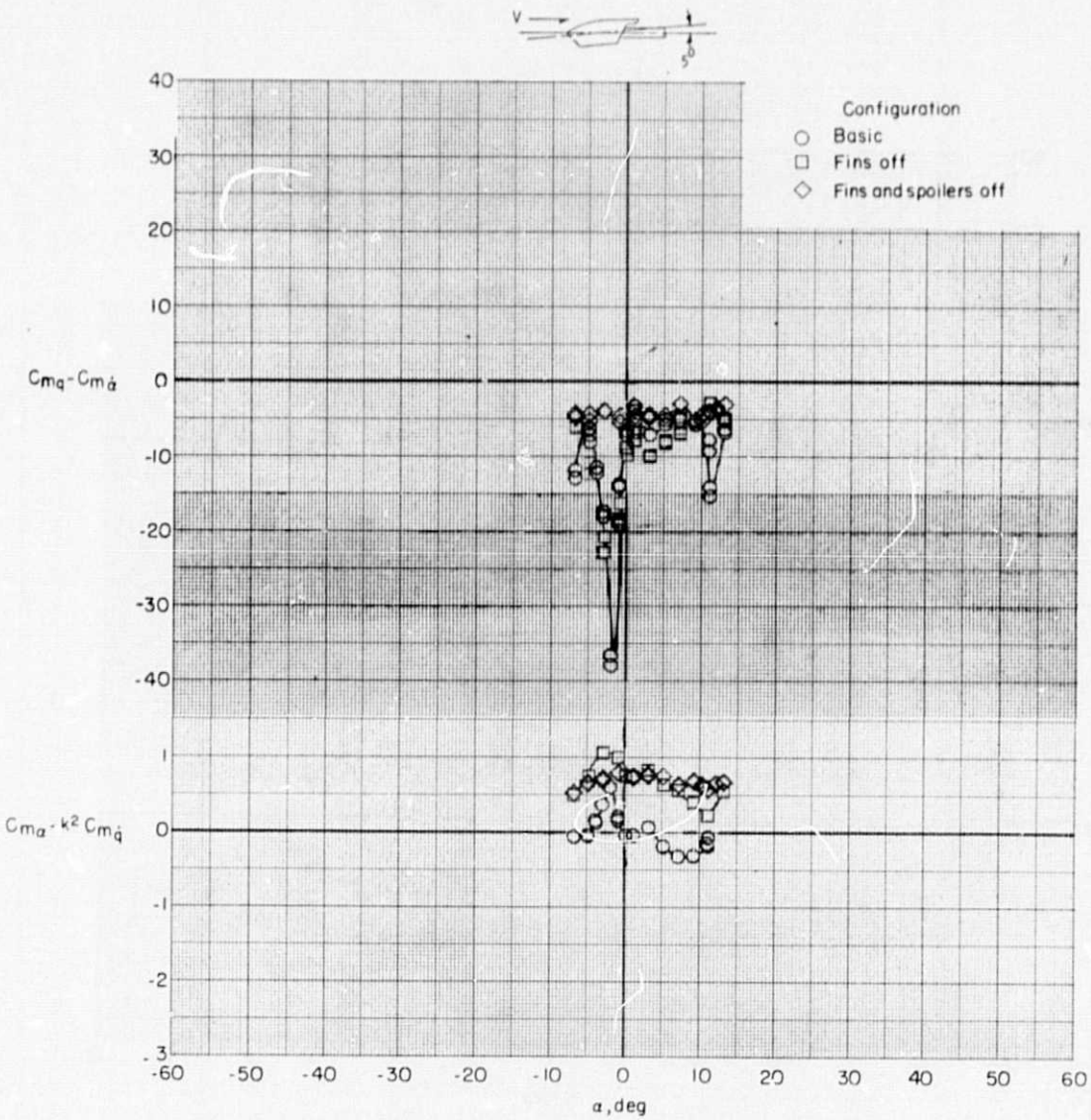

(a) M = 1.5

Figure 8.- Effect of component build-up on longitudinal dynamic stability characteristics, $\theta = +5^0$.

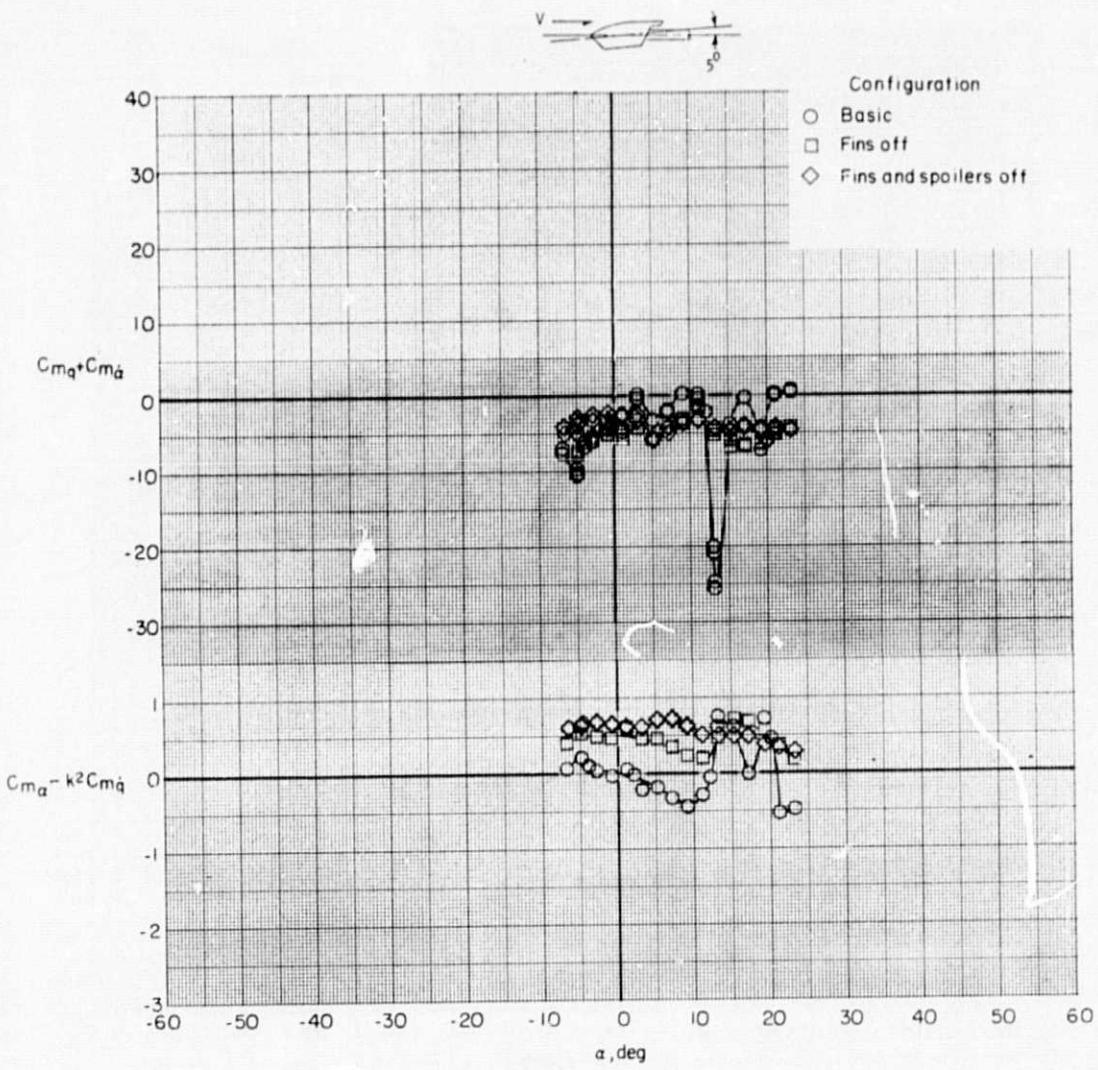

(b) M = 1.8

Figure 8.- Continued.

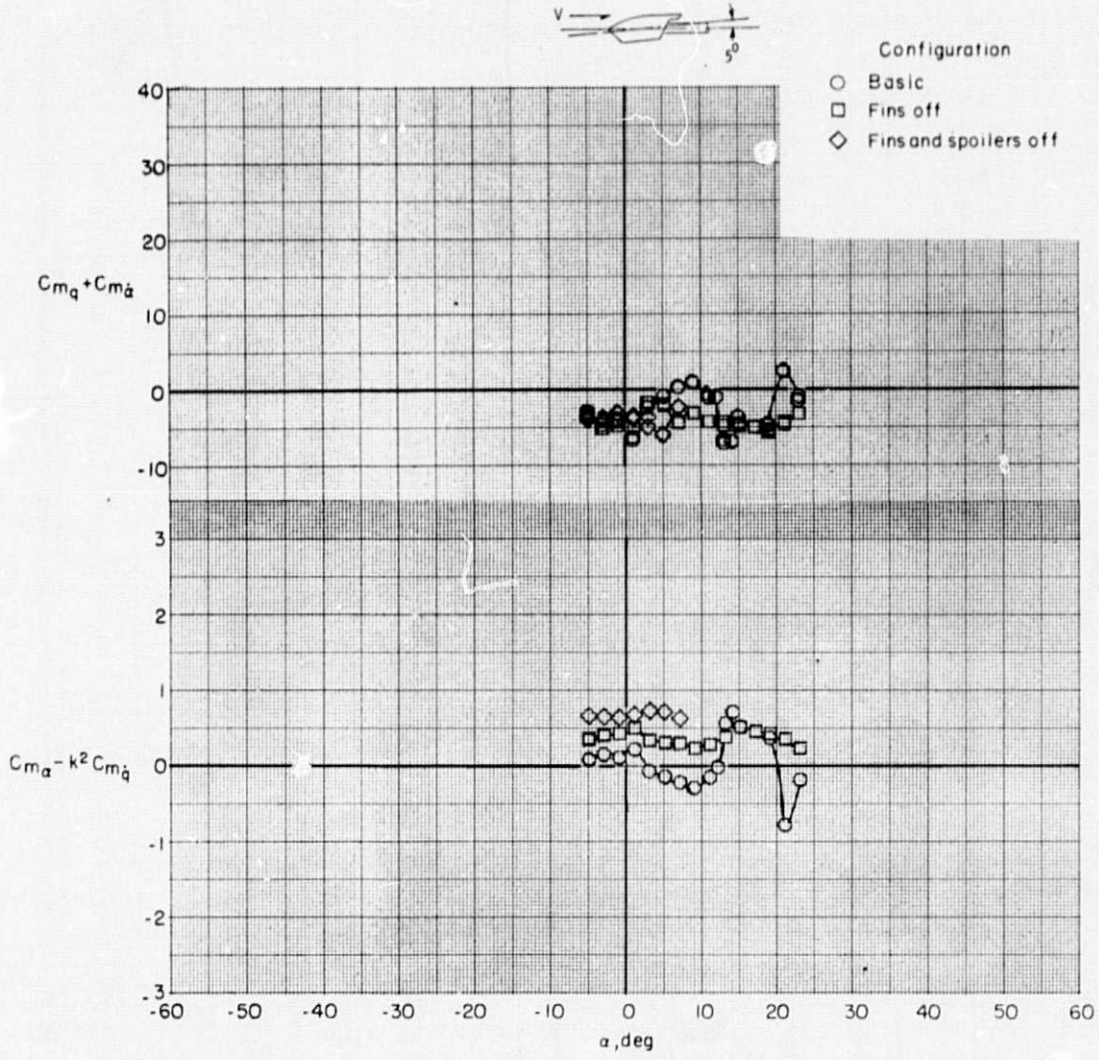

(c) M = 2.16

Figure 8. - Concluded.

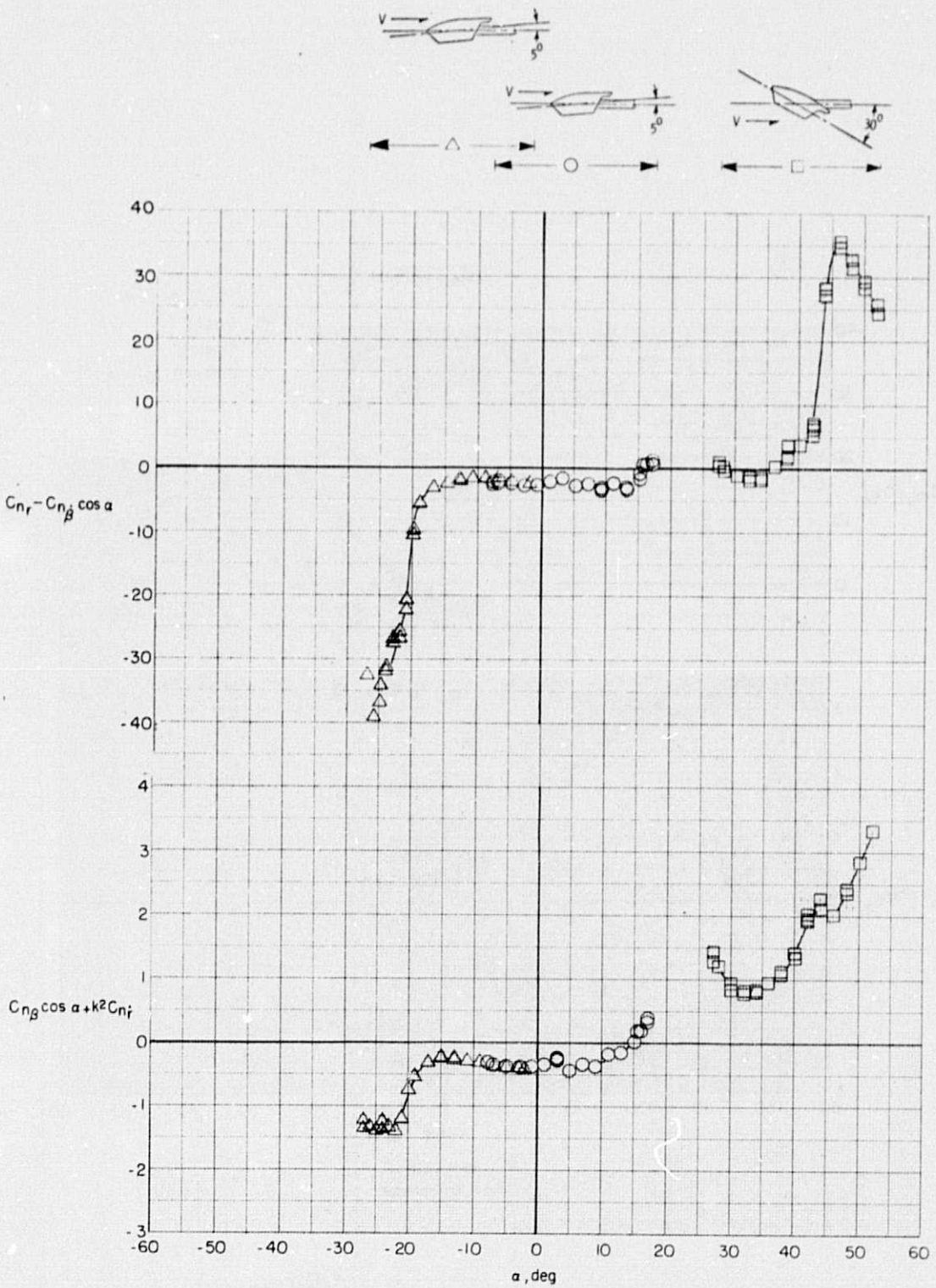

(a) M = 0.4

Figure 9.- Variation of lateral dynamic stability characteristics in yaw with mean angle of attack.

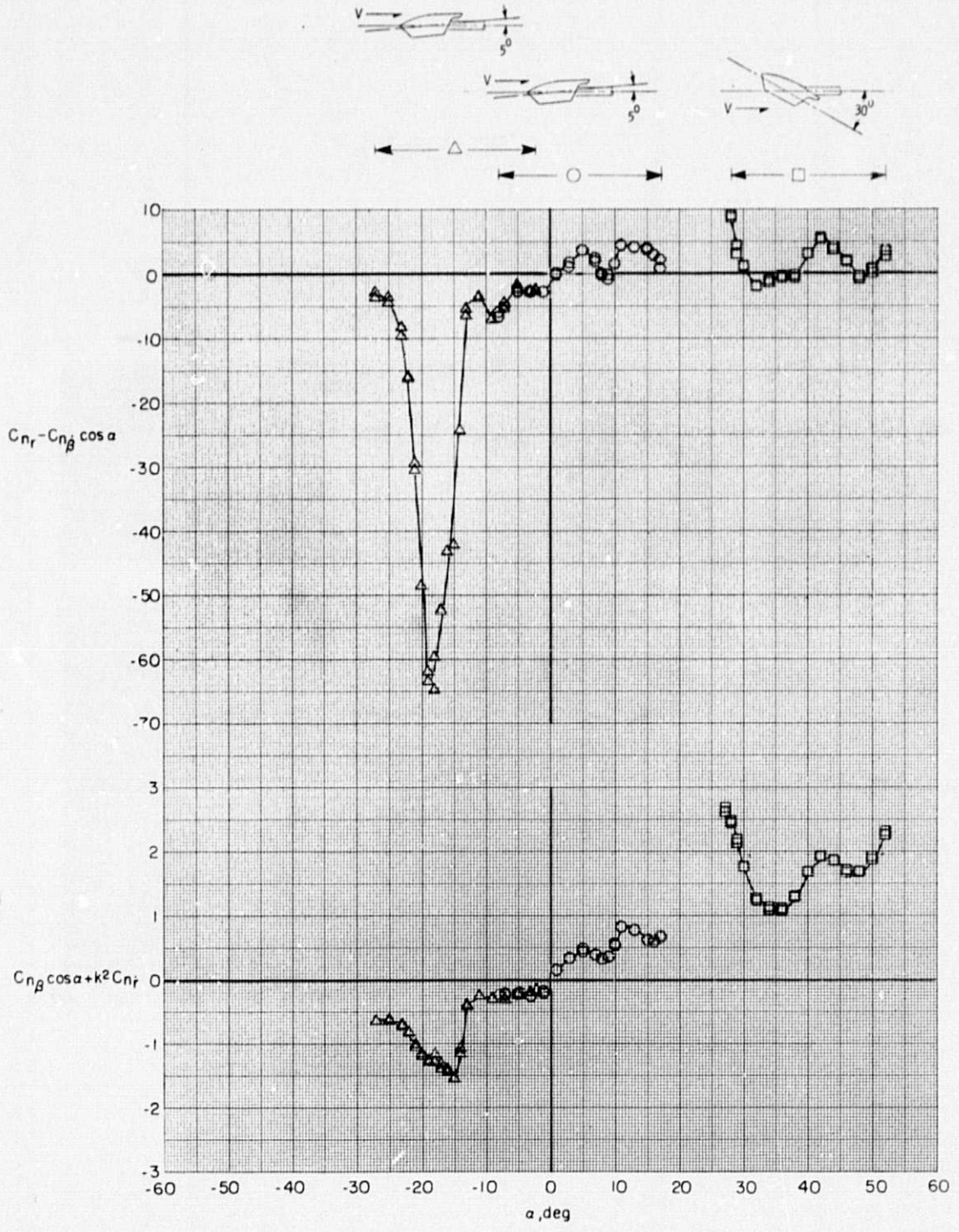

(b) M = 0.8

Figure 9.- Continued.

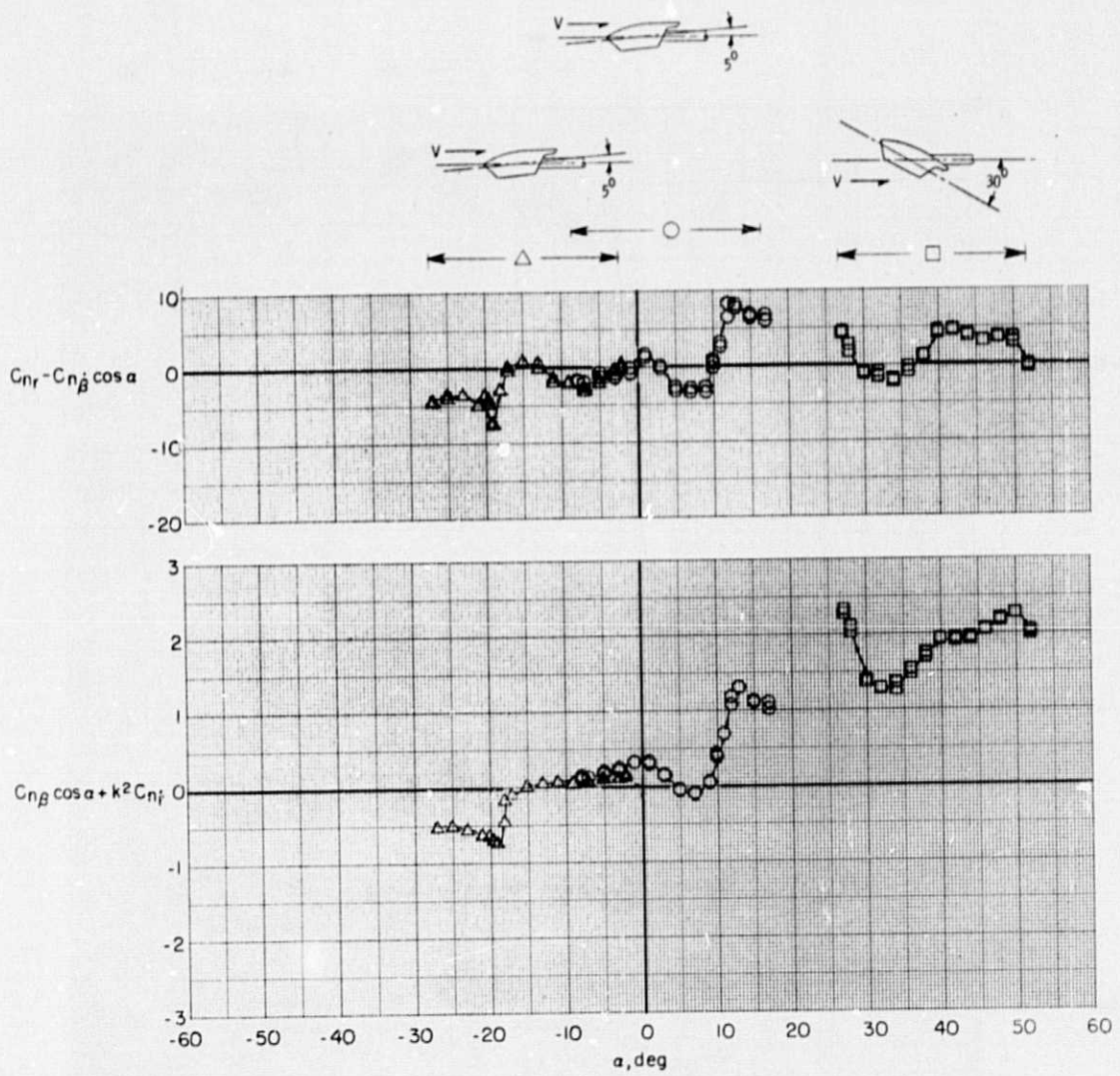

(c) M = 0.95

Figure 9.- Continued.

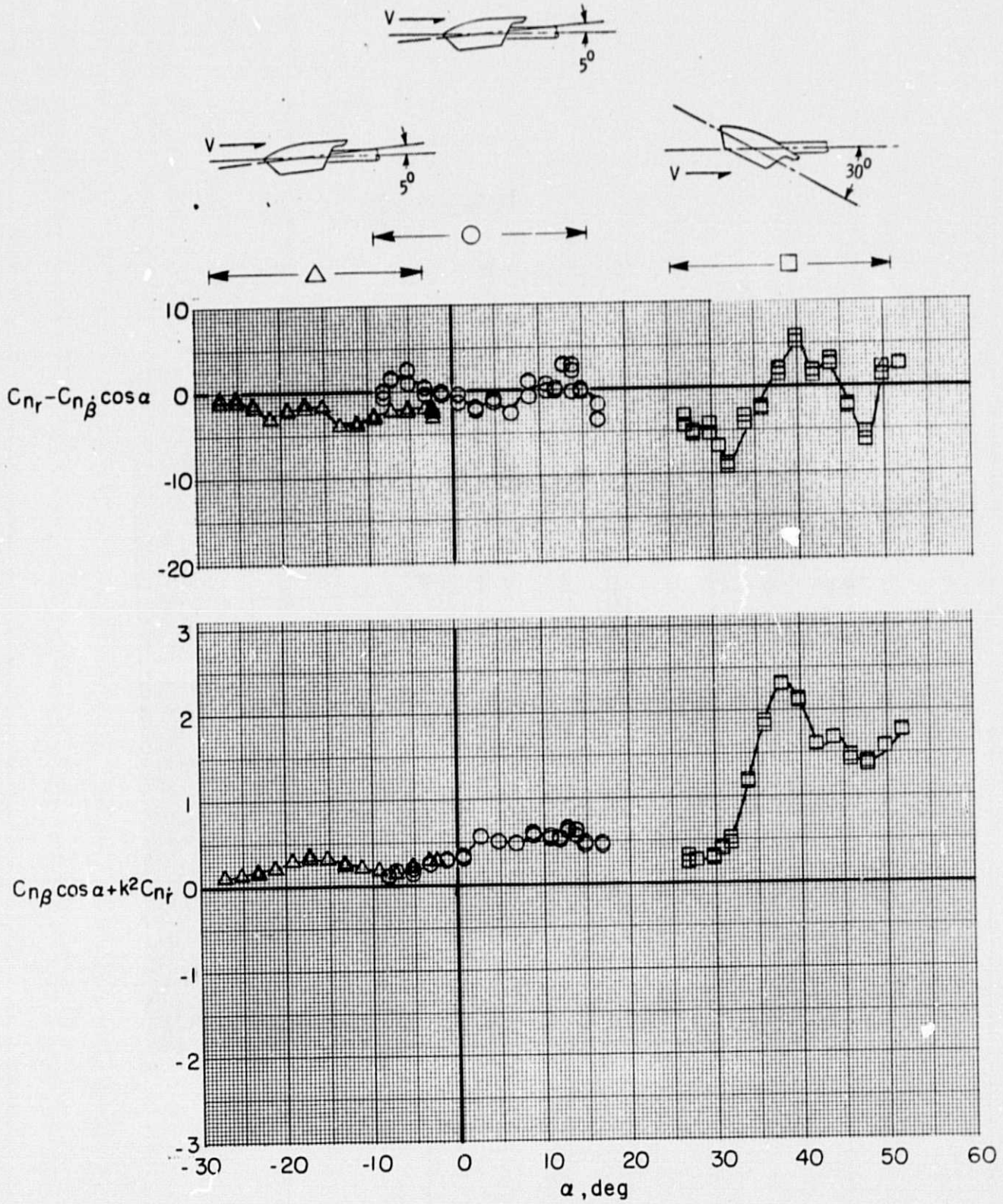

(e) M = 1.2

Figure 9.- Continued.

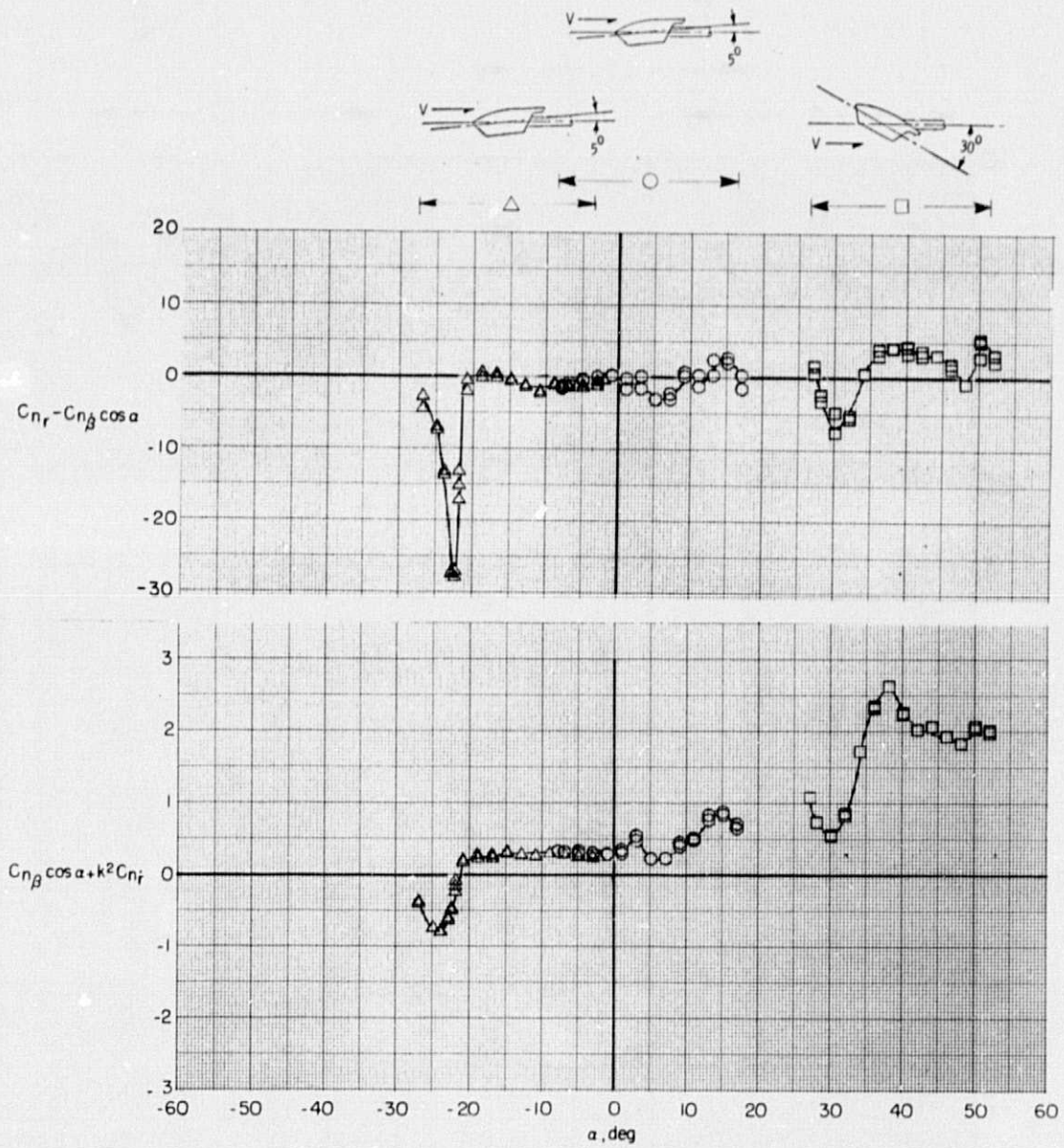

(d) M = 1.03

Figure 9.- Continued.

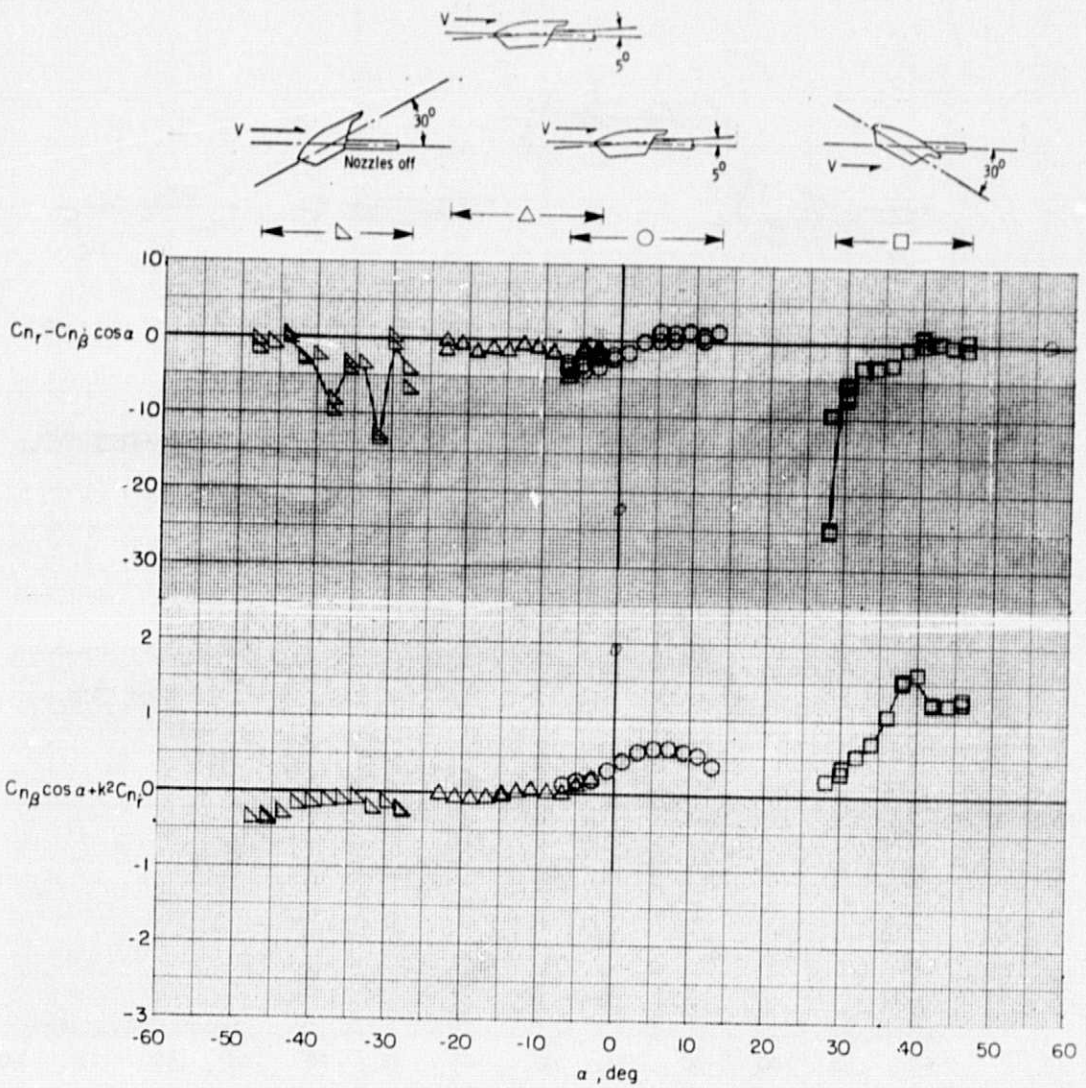

(f) M = 1.5

Figure 9.- Continued.

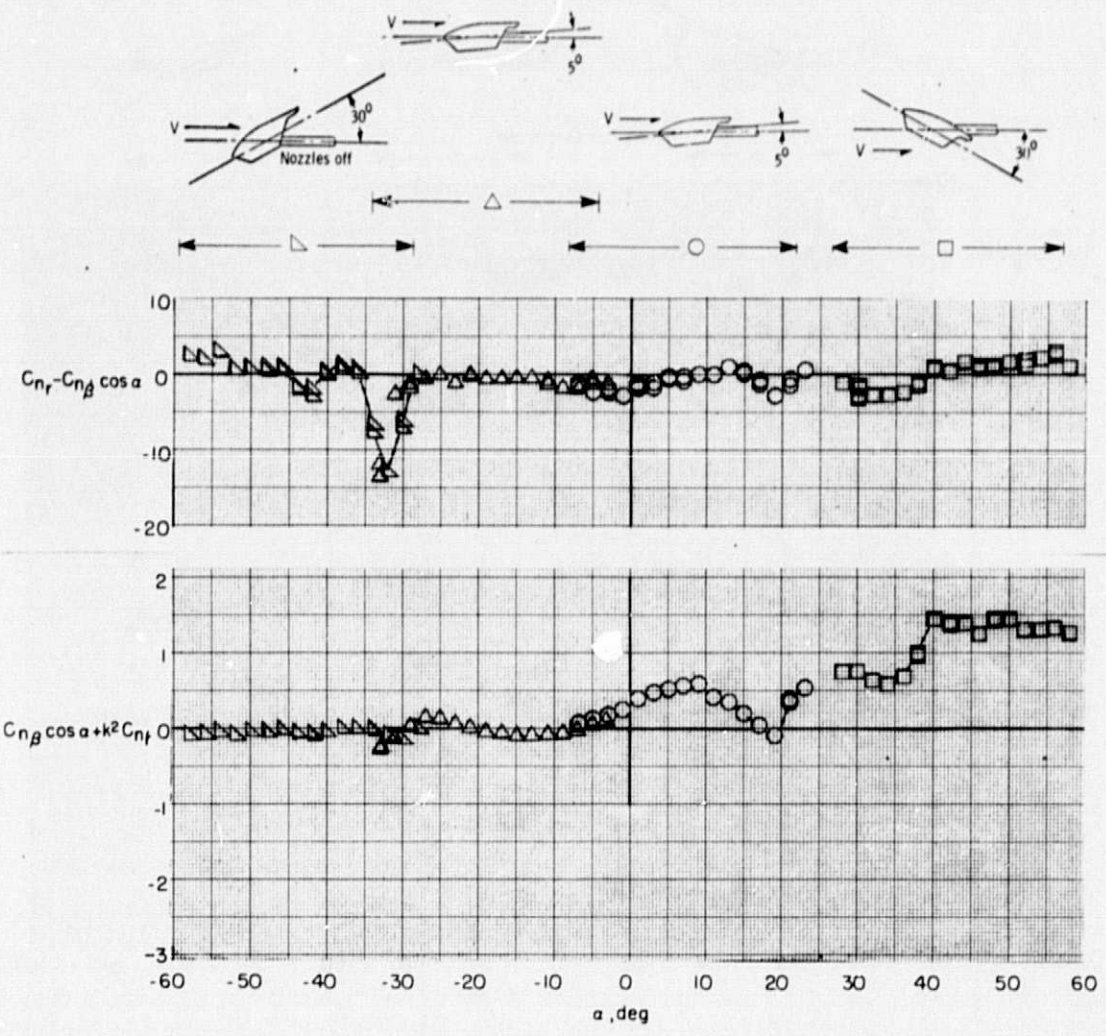

(g) M = 1.8

Figure 9.- Continued.

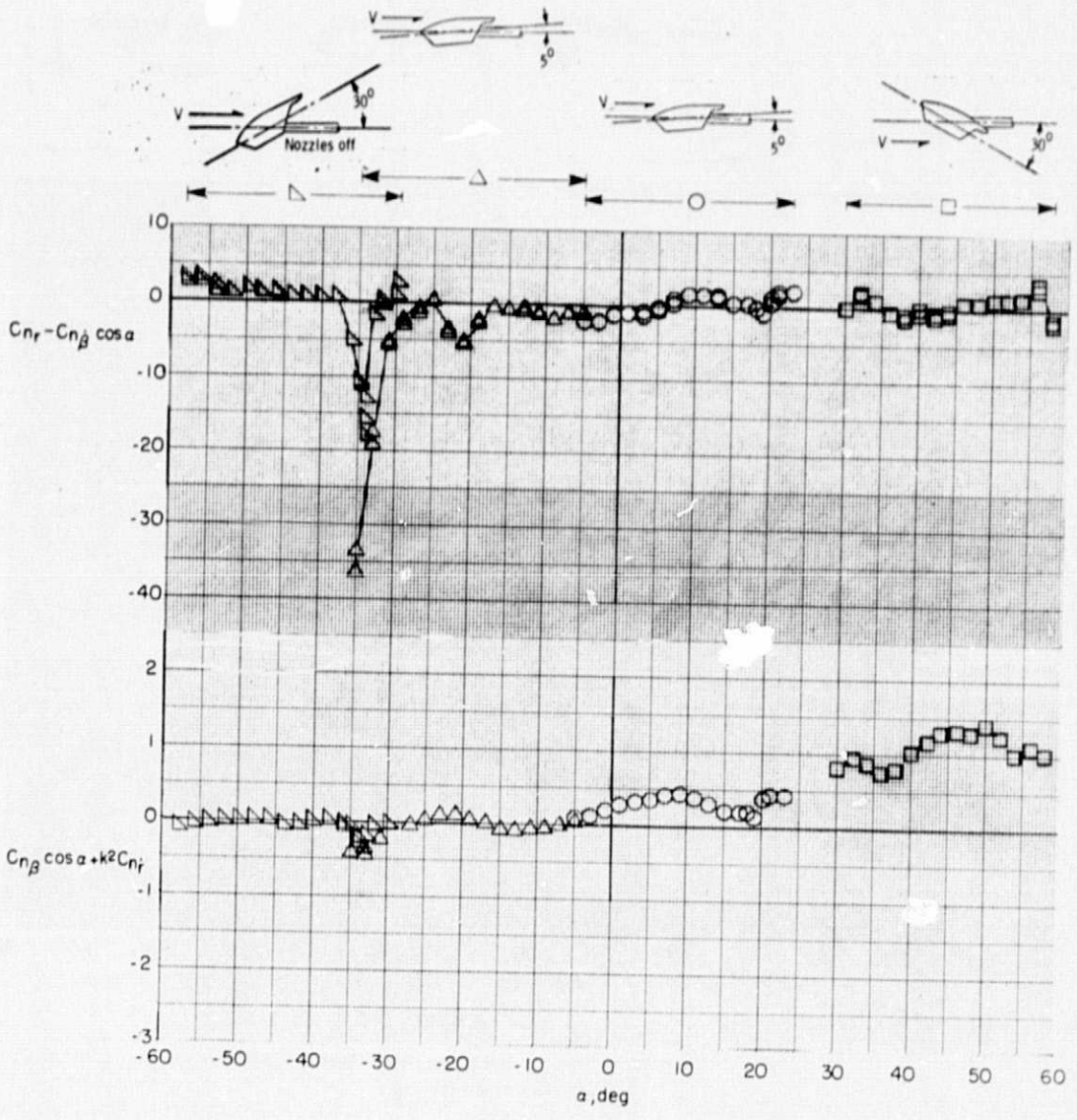

(h) M = 2.16

Figure 9. - Concluded.

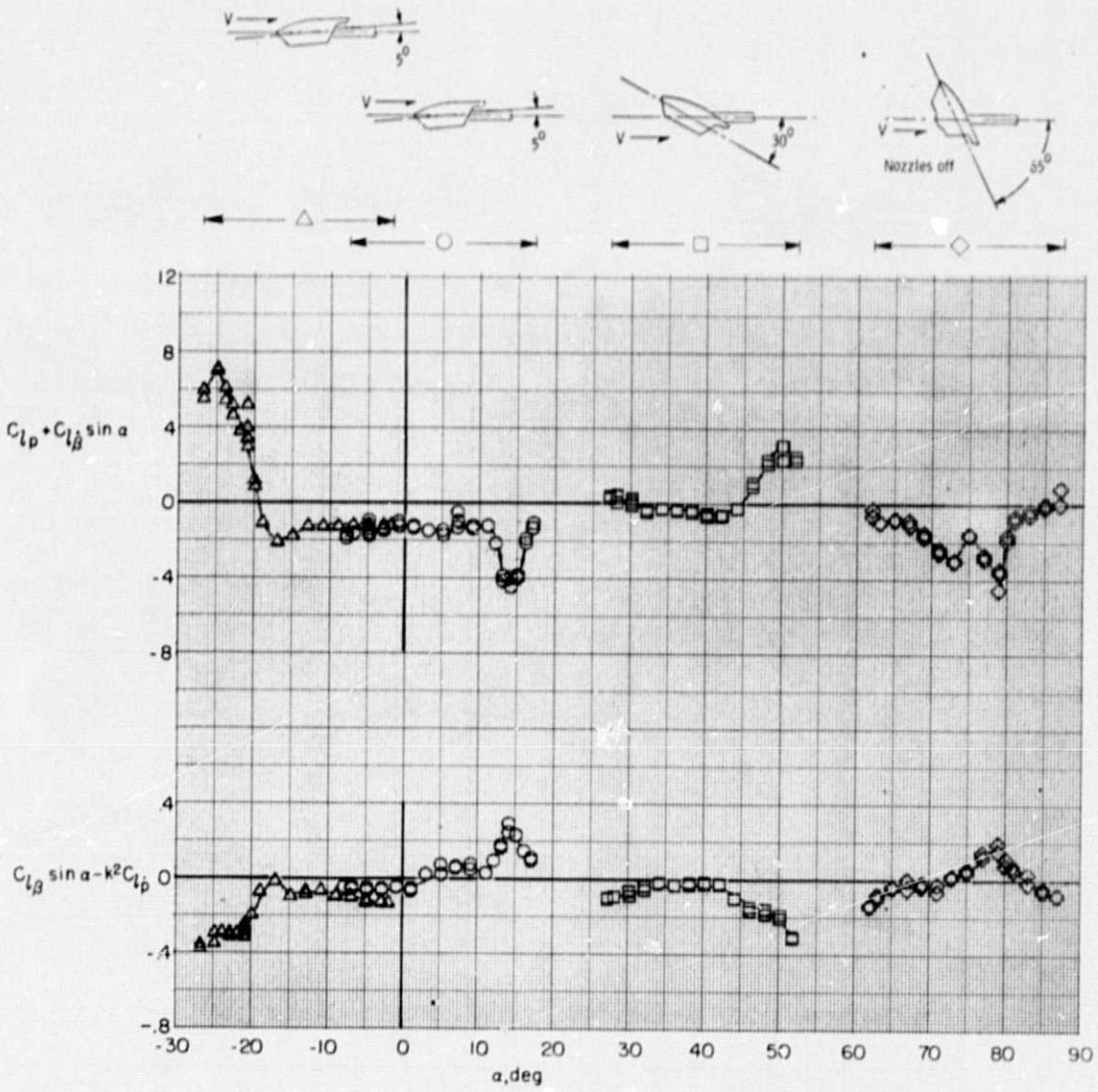

(a) M = 0.4

Figure 10.- Variation of dynamic stability characteristics in roll with mean angle of attack, nozzles on and off.

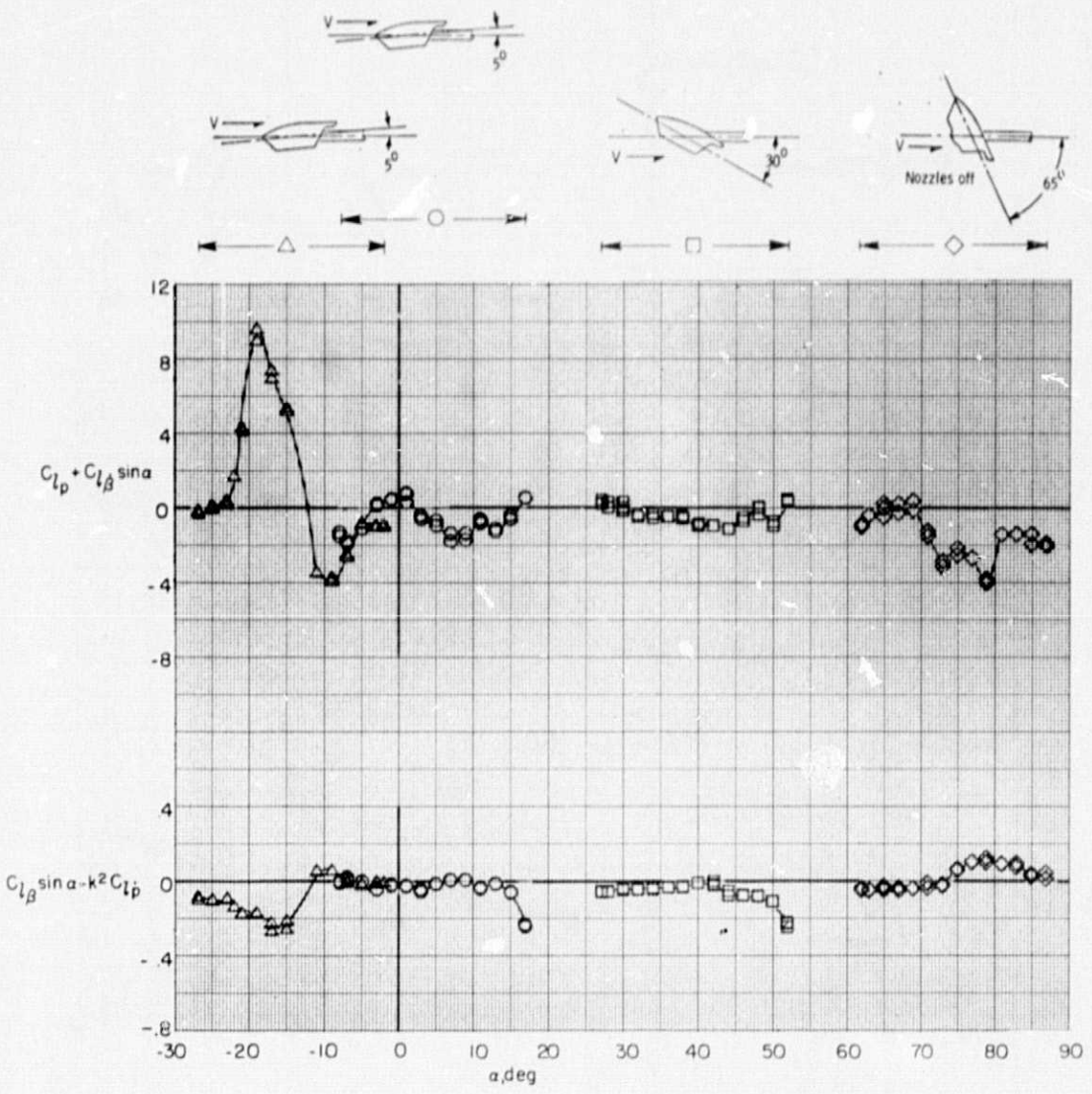

(b) M = 0.8

Figure 10. - Continued.

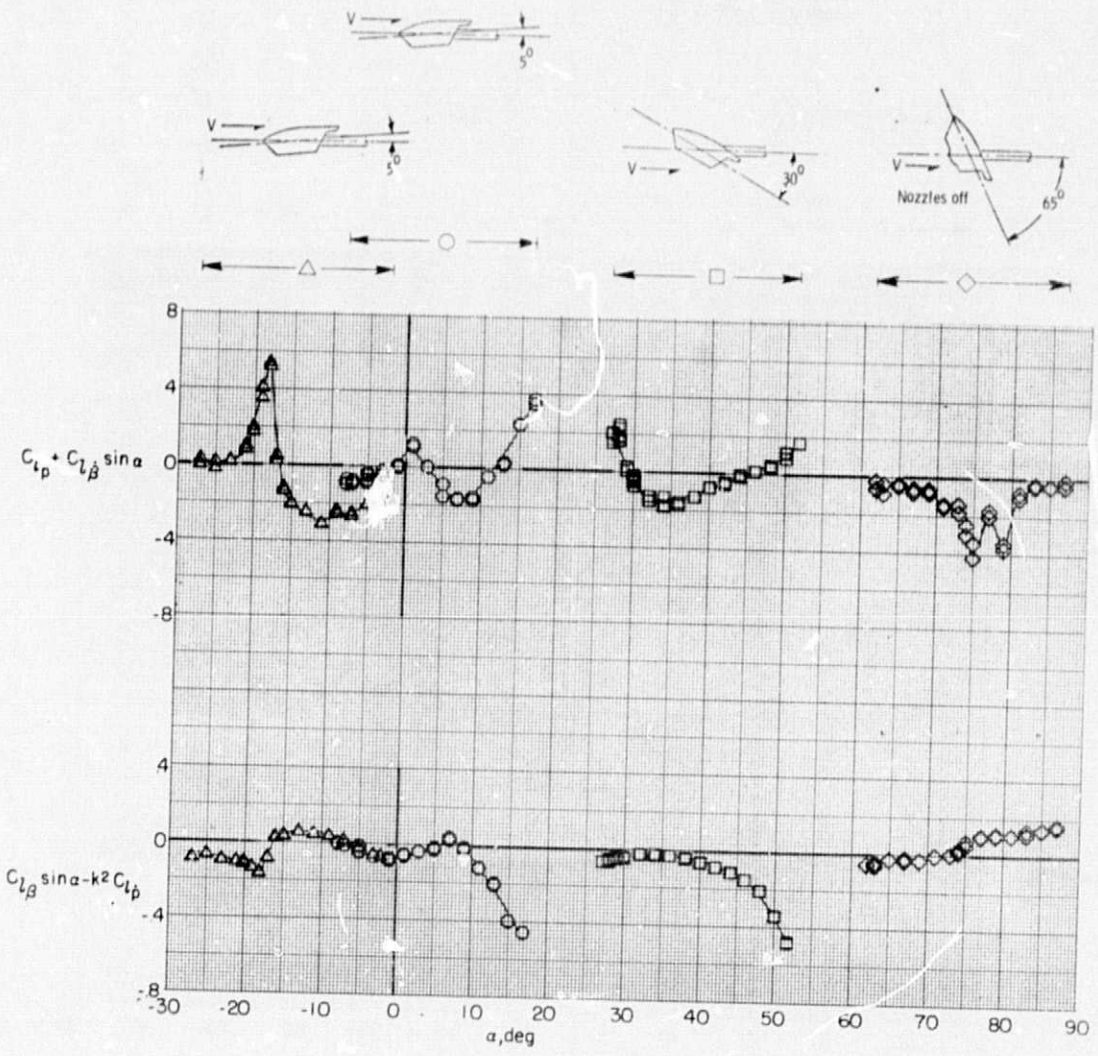

(c) M = 0.95

Figure 10. - Continued.

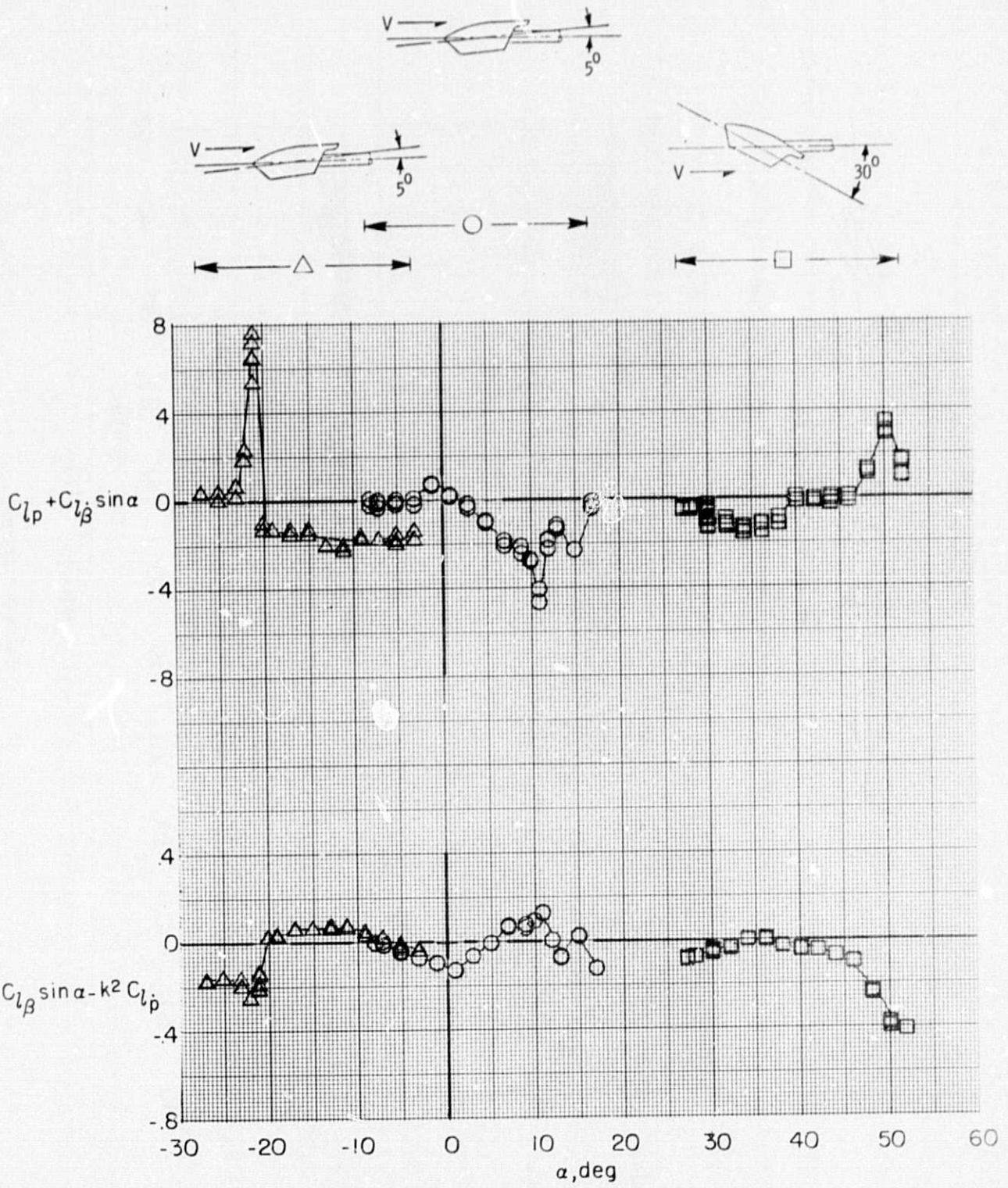

(d) M = 1.03

Figure 10. - Continued.

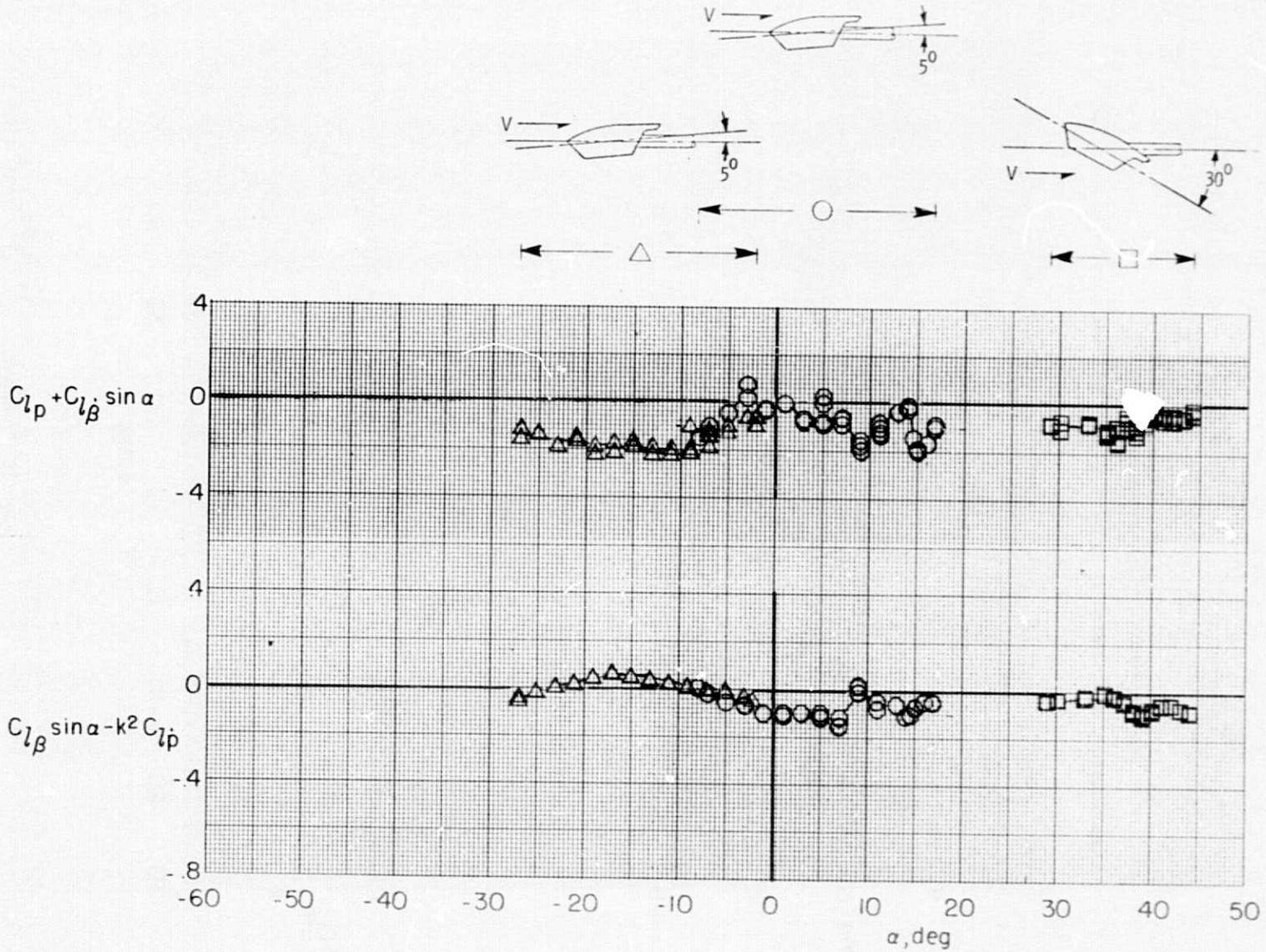

(e) M = 1.2

Figure 10. - Concluded.